



IRN TERASCALE

Rekindling s-Wave Dark Matter Annihilation Below 10 GeV with Breit-Wigner Effects

arXiv:2503.08897

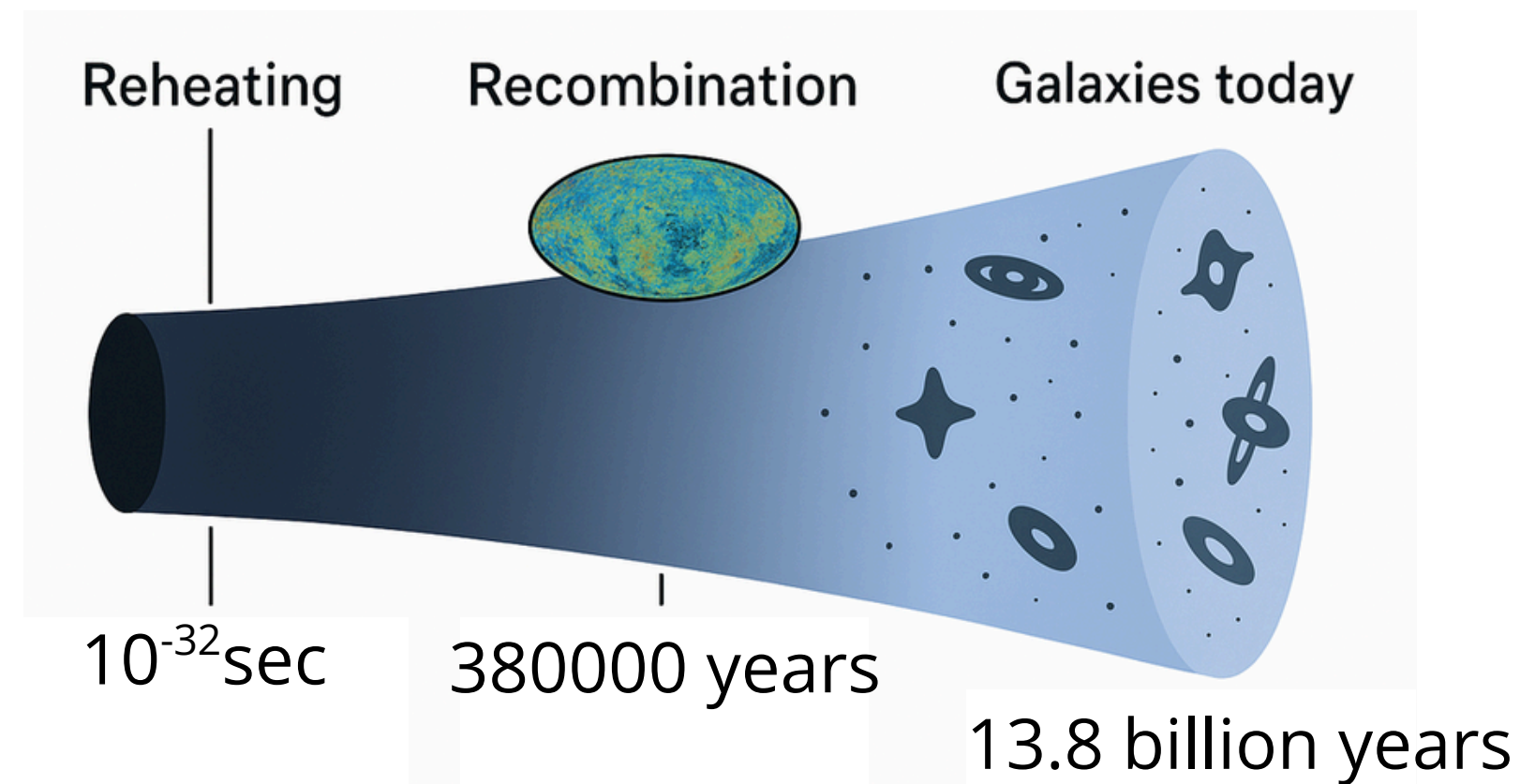
Geneviève Bélanger, Sreemanti Chakraborti, Cédric Delaunay, Margaux Jomain

me ↙

Introduction

Dark Matter (DM): several traces along the Universe

- After reheating, freeze-in or freeze-out \rightarrow relic density
- At recombination: traces in Cosmic Microwave Background (CMB)
- Present in galaxies today: potential traces ?



Introduction

Dark Matter (DM): several traces along the Universe

- After reheating, freeze-in or freeze-out \rightarrow relic density
- At recombination: traces in Cosmic Microwave Background (CMB)
- Present in galaxies today: potential traces ?

In this work: Focus on **thermal s-wave DM** with a mass **below 10 GeV**.

1. Cosmological context \rightarrow this DM is excluded in standard case
2. Introduction of **resonance** to rekindle it
3. **CMB** constraints on resonant models
4. Possibility to detect DM with **indirect detection**

model-independant

Cosmological context

The cosmological context

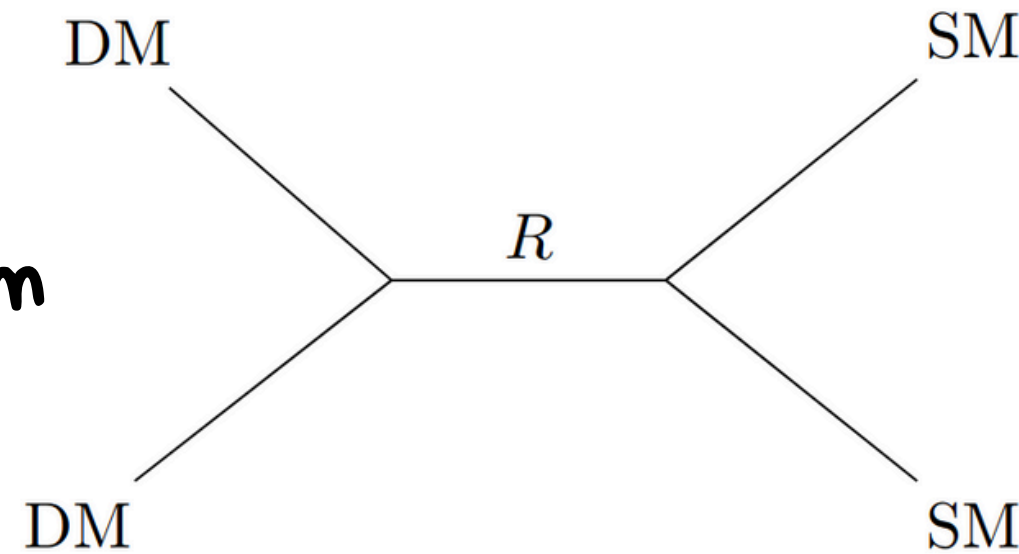
Thermal Dark Matter: Freeze-out

hypotheses:

FLRW metric

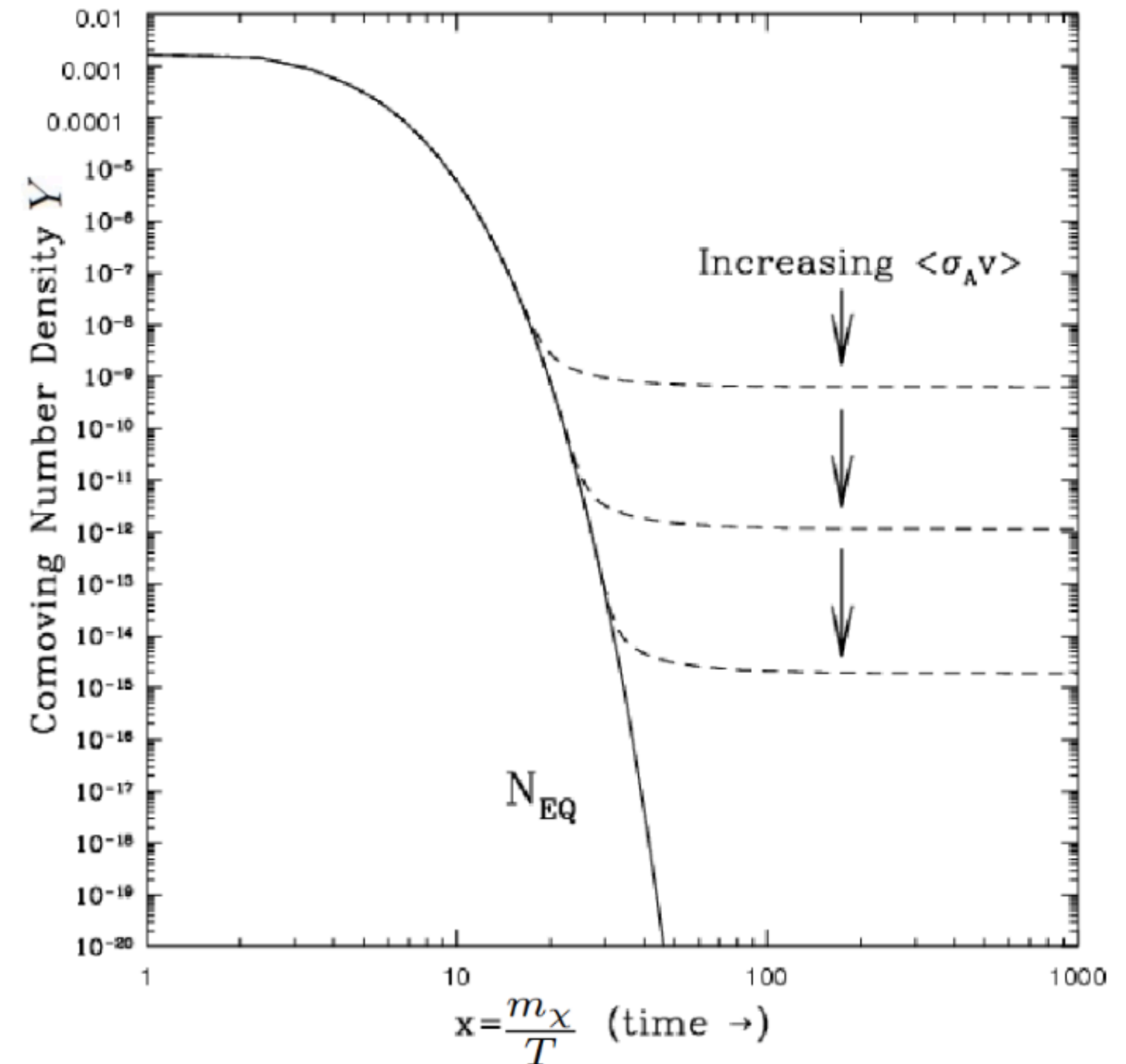
CP invariance

kinetic equilibrium




Boltzmann equation:

$$\frac{dY}{dx} = - \sqrt{\frac{\pi}{45G}} \frac{m}{x^2} g^{*1/2} \langle \sigma v_{M\phi l} \rangle (Y^2 - Y_{eq}^2)$$



s-wave annihilation cross section

velocity dispersion


$$\langle \sigma v \rangle = c_0 + c_1 v^2 + c_2 v^4 + \dots + c_n v^{2n}$$

s-wave annihilation cross section

velocity dispersion

$$\langle \sigma v \rangle = c_0 + c_1 v^2 + c_2 v^4 + \dots + c_n v^{2n}$$

$\rightarrow = 0 \rightarrow \text{p-wave (or d-wave,...)}$

$\rightarrow \neq 0 \rightarrow \text{s-wave}$

s-wave annihilation cross section

$$\langle \sigma v \rangle = c_0 + c_1 v^2 + c_2 v^4 + \dots + c_n v^{2n}$$

velocity dispersion

$= 0 \rightarrow$ p-wave (or d-wave,...)

$\neq 0 \rightarrow$ s-wave

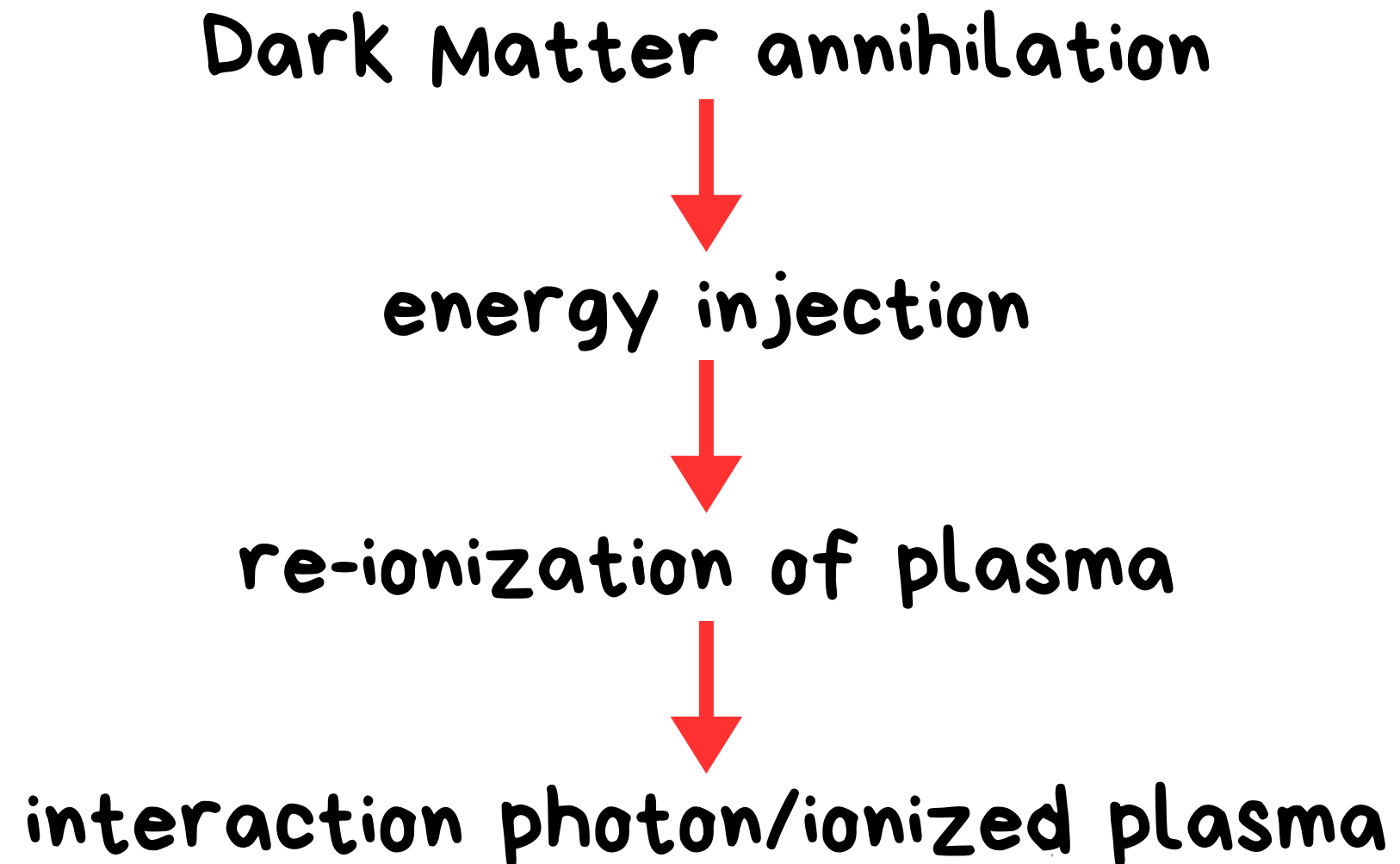
$$v_{\text{FO}} \simeq 10^{-1} c$$

$$v_{\text{CMB}} \simeq 10^{-8} c$$

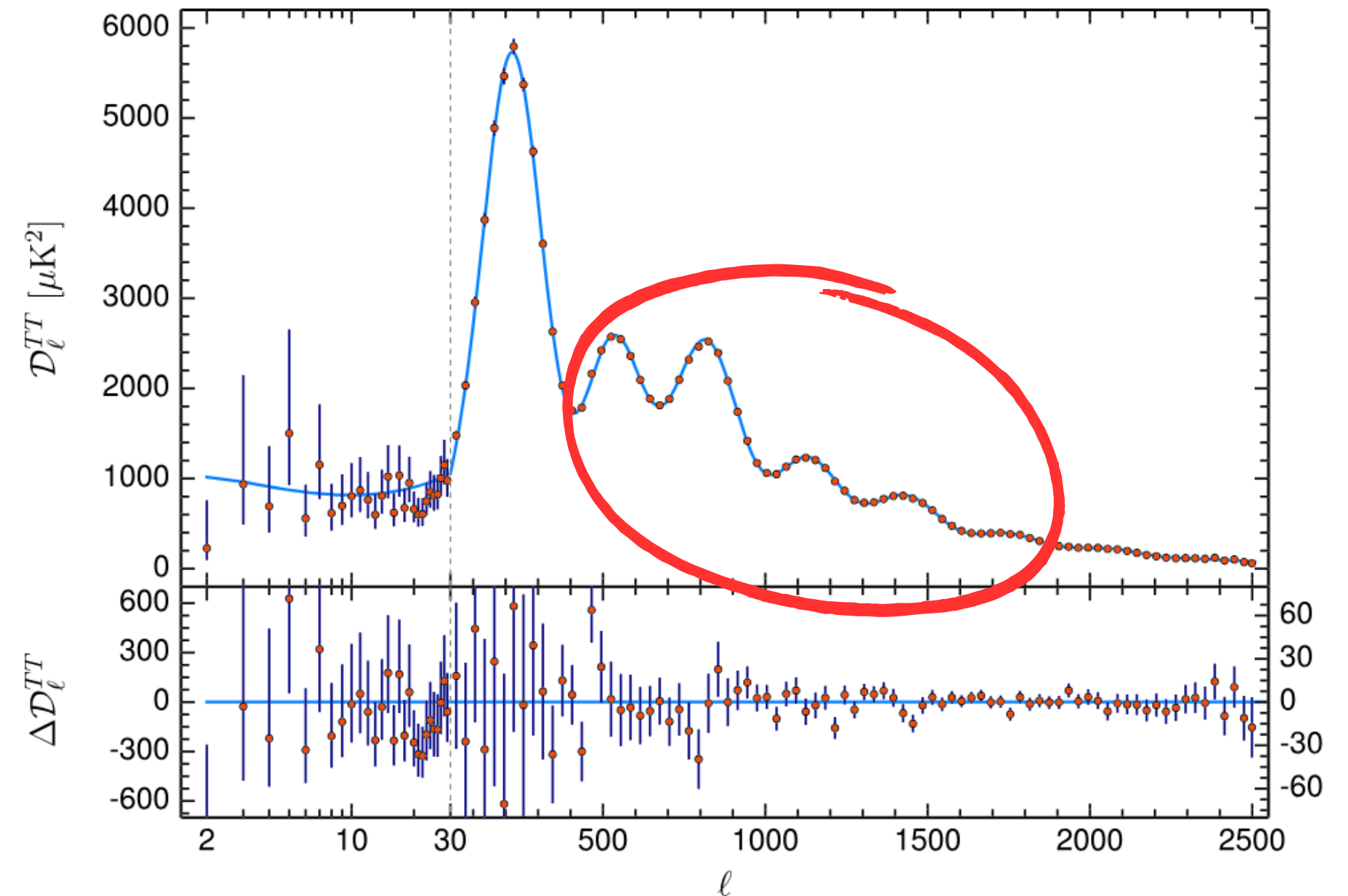


Constraints on Dark Matter

CMB Constraints



S. Dodelson, F. Schmidt : Modern Cosmology



- CMB: strong constraints on annihilation cross section (ACS) for $m_\chi < 10\text{GeV}$
 - s Wave: ACS not very different during freeze out and during CMB
- Most of the time, ACS that reproduces relic density = excluded by CMB

Almost every s-wave light DM model excluded

- CMB: strong constraints on annihilation cross section (ACS) for $m_\chi < 10\text{GeV}$
 - s Wave: ACS not very different during freeze out and during CMB
- Most of the time, ACS that reproduces relic density = excluded by CMB

Almost every s-wave light DM model excluded

→ Resonant models can evade

Goal of this work

Being **model-independent**, we show that a narrow resonances can reproduce the **relic density** evading **CMB constraints**, potentially allowing to detect s-wave DM annihilation in the **present Universe**

What is a resonance ?

Resonance

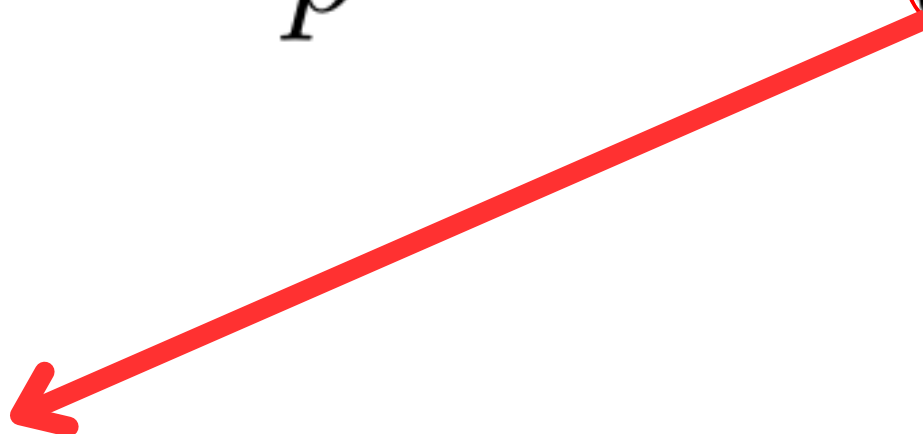
Breit-Wigner cross section

$$\sigma_{\chi\chi\rightarrow f} = g_{\chi}g_{\text{SM}}\frac{4\pi\omega}{p^2}B_{\chi}B_f\frac{m_R^2\Gamma_R^2}{(s-m_R^2)^2+m_R^2\Gamma_R^2}$$

Resonance

Breit-Wigner cross section

$$\sigma_{\chi\chi\rightarrow f} = g_{\chi}g_{\text{SM}}\frac{4\pi\omega}{p^2}B_{\chi}B_f\frac{m_R^2\Gamma_R^2}{(s - m_R^2)^2 + m_R^2\Gamma_R^2}$$

$$4m_{\chi}^2 (1 + v^2 + o(v^4))$$


Resonance

Breit-Wigner cross section

$$\sigma_{\chi\chi\rightarrow f} = g_\chi g_{\text{SM}} \frac{4\pi\omega}{p^2} B_\chi B_f \frac{m_R^2 \Gamma_R^2}{(s - m_R^2)^2 + m_R^2 \Gamma_R^2}$$

$$4m_\chi^2 (1 + v^2 + o(v^4))$$

$$= 0 \text{ for } m_R^2 = 4m_\chi^2 (1 + v^2)$$

$$\Leftrightarrow \frac{m_R^2 - 4m_\chi^2}{4m_\chi^2} = v^2$$

Resonance

Breit-Wigner cross section

$$\sigma_{\chi\chi \rightarrow f} = g_\chi g_{\text{SM}} \frac{4\pi\omega}{p^2} B_\chi B_f \frac{m_R^2 \Gamma_R^2}{(s - m_R^2)^2 + m_R^2 \Gamma_R^2}$$

$\xrightarrow{\text{red arrow}} = 0 \text{ for } m_R^2 = 4m_\chi^2 (1 + v^2)$

$\xrightarrow{\text{red arrow}} 4m_\chi^2 (1 + v^2 + o(v^4))$

$\Leftrightarrow \frac{m_R^2 - 4m_\chi^2}{4m_\chi^2} = v^2$

ϵ_R

Resonance

Breit-Wigner cross section

$$\gamma_R \equiv \frac{m_R^2 \Gamma_R^2}{4m_\chi^2}$$

$$\sigma_{\chi\chi \rightarrow f} = g_\chi g_{\text{SM}} \frac{4\pi\omega}{p^2} B_\chi B_f \frac{m_R^2 \Gamma_R^2}{(s - m_R^2)^2 + m_R^2 \Gamma_R^2}$$

= 0 for $m_R^2 = 4m_\chi^2 (1 + v^2)$

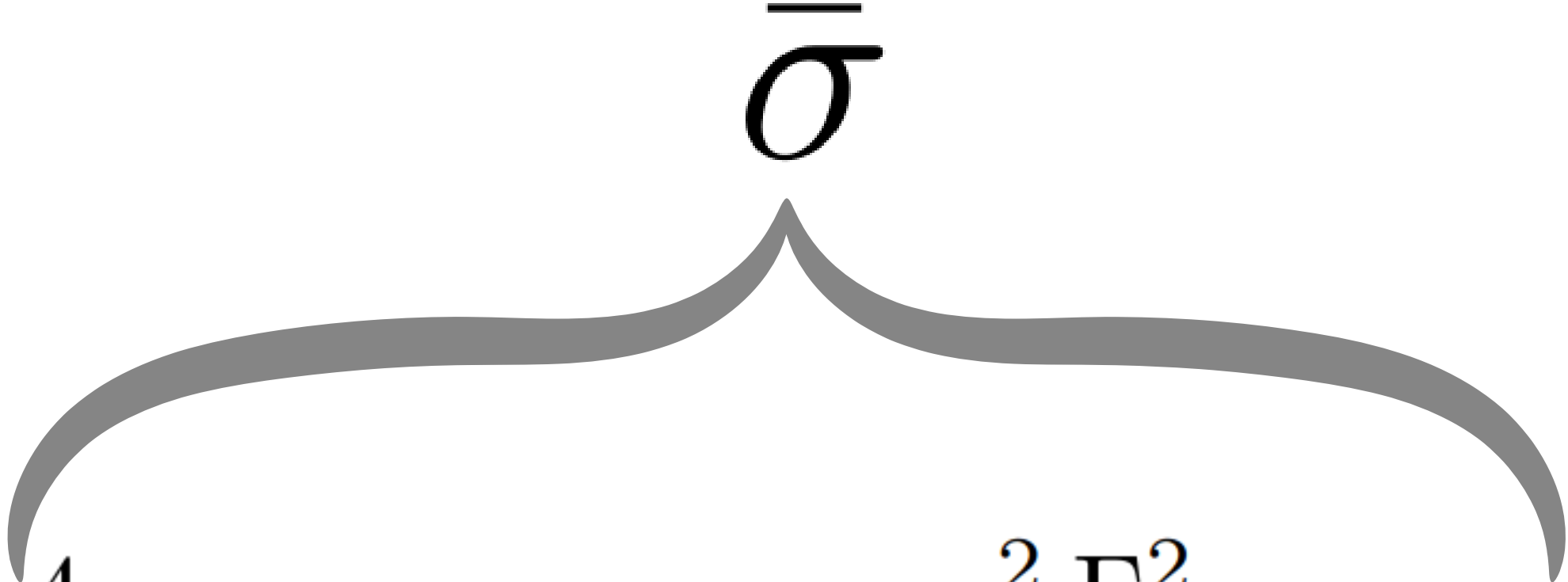
$\Leftrightarrow \frac{m_R^2 - 4m_\chi^2}{4m_\chi^2} = v^2$

ϵ_R

$4m_\chi^2 (1 + v^2 + o(v^4))$

Resonance

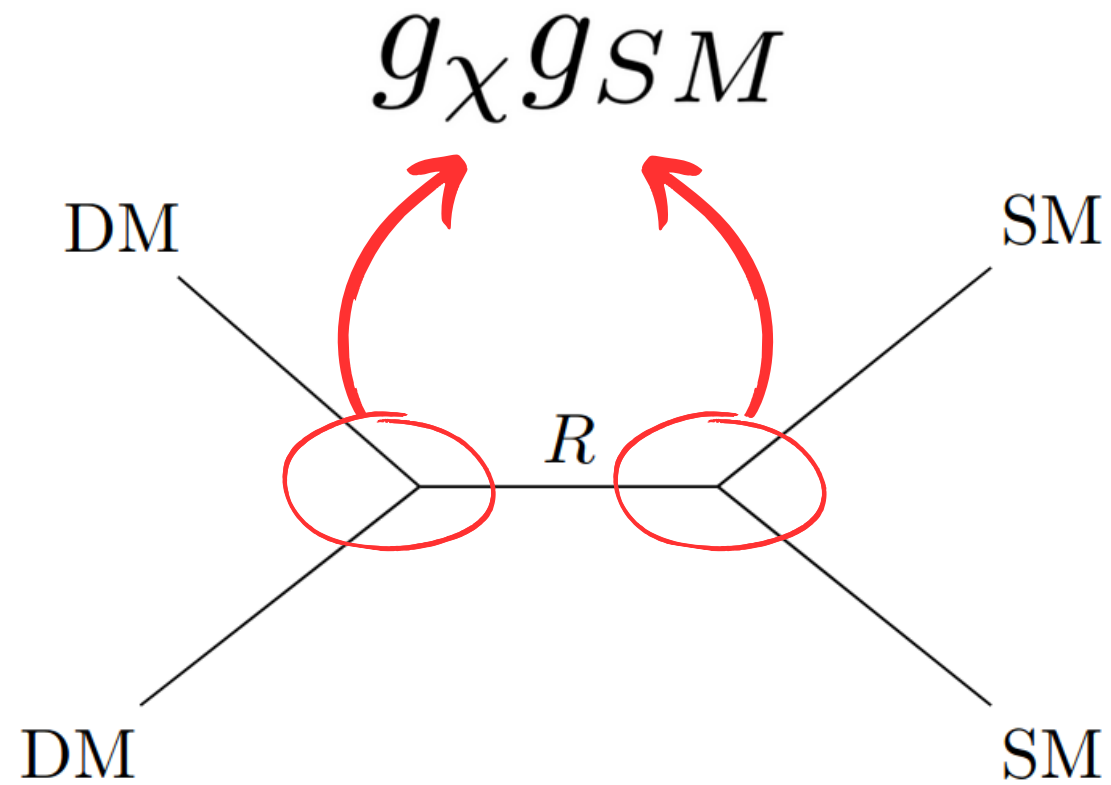
Breit-Wigner cross section


$$\sigma_{\chi\chi\rightarrow f} = g_{\chi}g_{\text{SM}}\frac{4\pi\omega}{p^2}B_{\chi}B_f\frac{m_R^2\Gamma_R^2}{(s-m_R^2)^2+m_R^2\Gamma_R^2}$$

Why a resonance ?

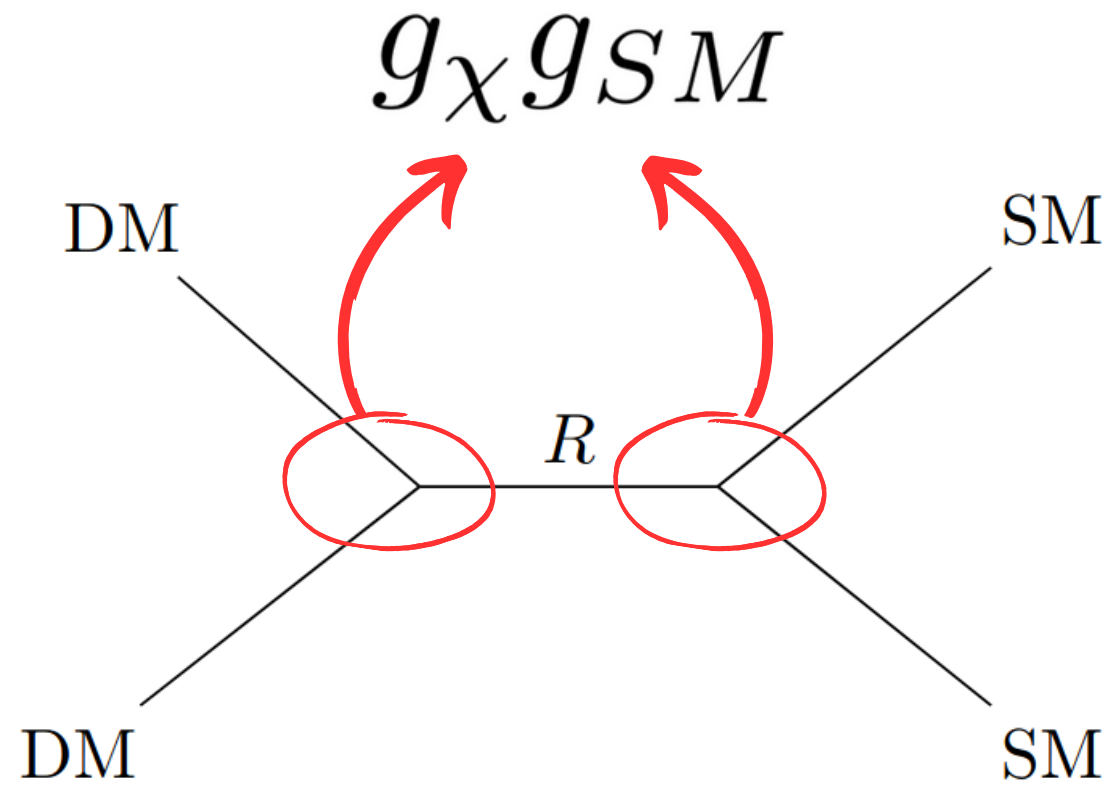
Resonance

$$\frac{1}{\Omega h^2} \propto \int \sigma_{\chi\chi \rightarrow f} = g_\chi g_{\text{SM}} \int \bar{\sigma}$$



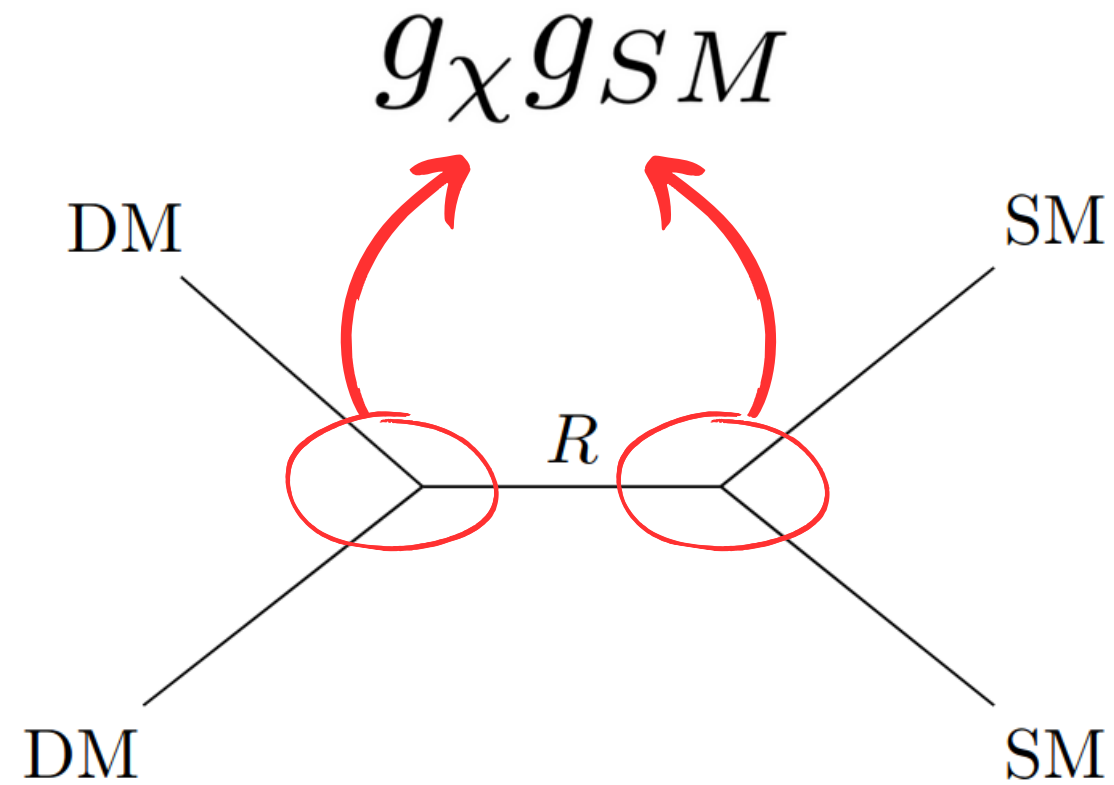
Resonance

$$\frac{1}{\Omega h^2} \propto \int \sigma_{\chi\chi \rightarrow f} = g_\chi g_{\text{SM}} \int \vec{\sigma}$$



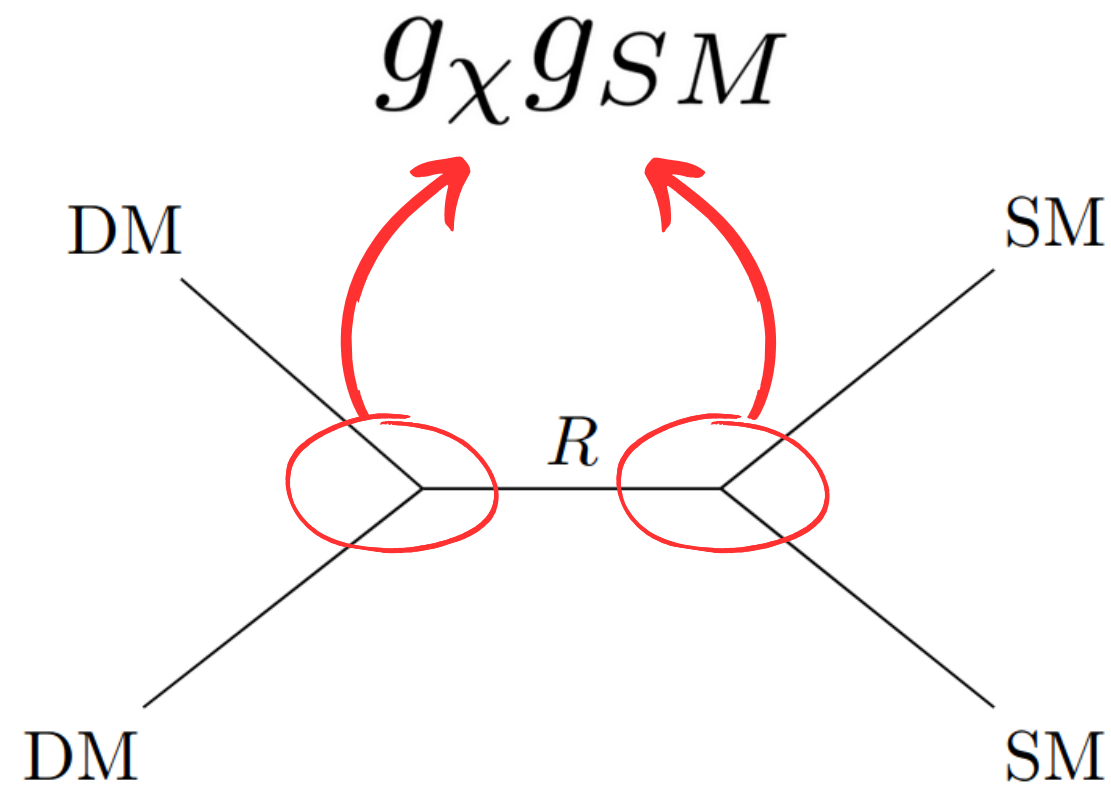
Resonance

$$\frac{1}{\Omega h^2} \propto \int \sigma_{\chi\chi \rightarrow f} = g_\chi g_{\text{SM}} \int \bar{\sigma}$$



Resonance

$$\frac{1}{\Omega h^2} \propto \int \sigma_{\chi\chi \rightarrow f} = g_\chi g_{\text{SM}} \int \bar{\sigma}$$

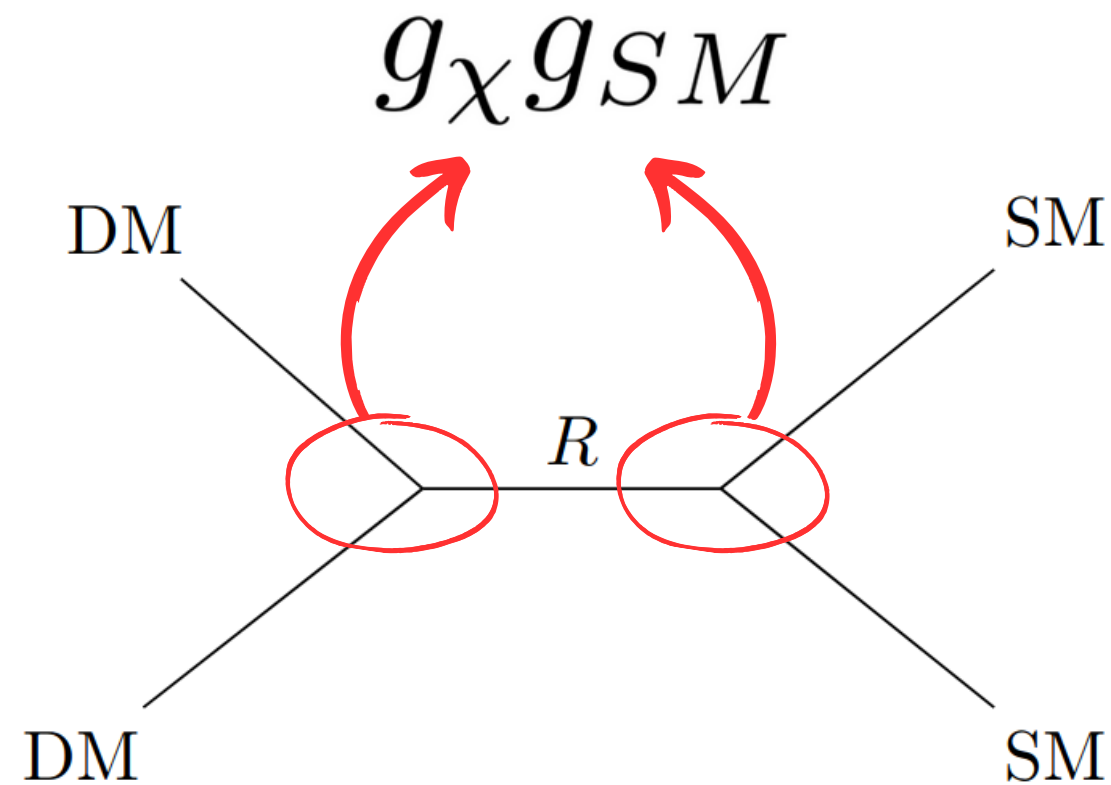


**During CMB epoch, not
boosted !**

$$g_\chi g_{\text{SM}} \bar{\sigma}_{\text{CMB}}$$

Resonance

$$\frac{1}{\Omega h^2} \propto \int \sigma_{\chi\chi \rightarrow f} = g_\chi g_{\text{SM}} \int \bar{\sigma}$$



During CMB epoch, not
boosted !

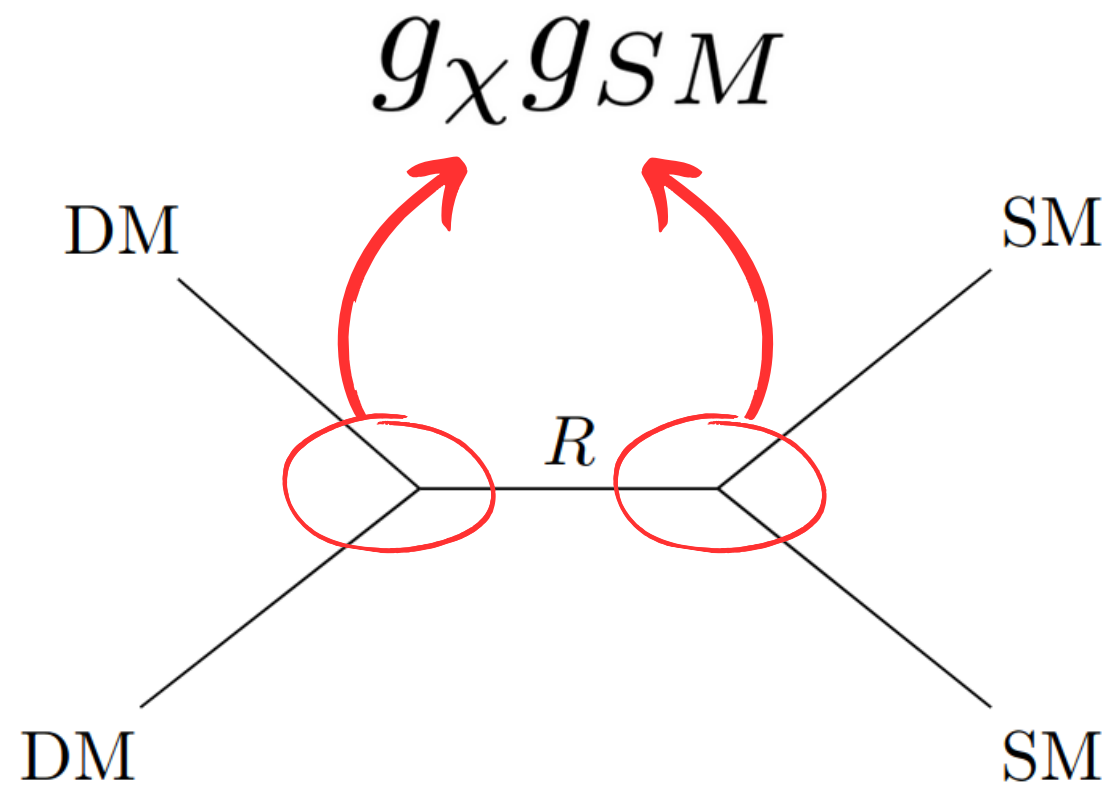
$$g_\chi g_{\text{SM}} \bar{\sigma}_{\text{CMB}}$$

Can escape the constraints

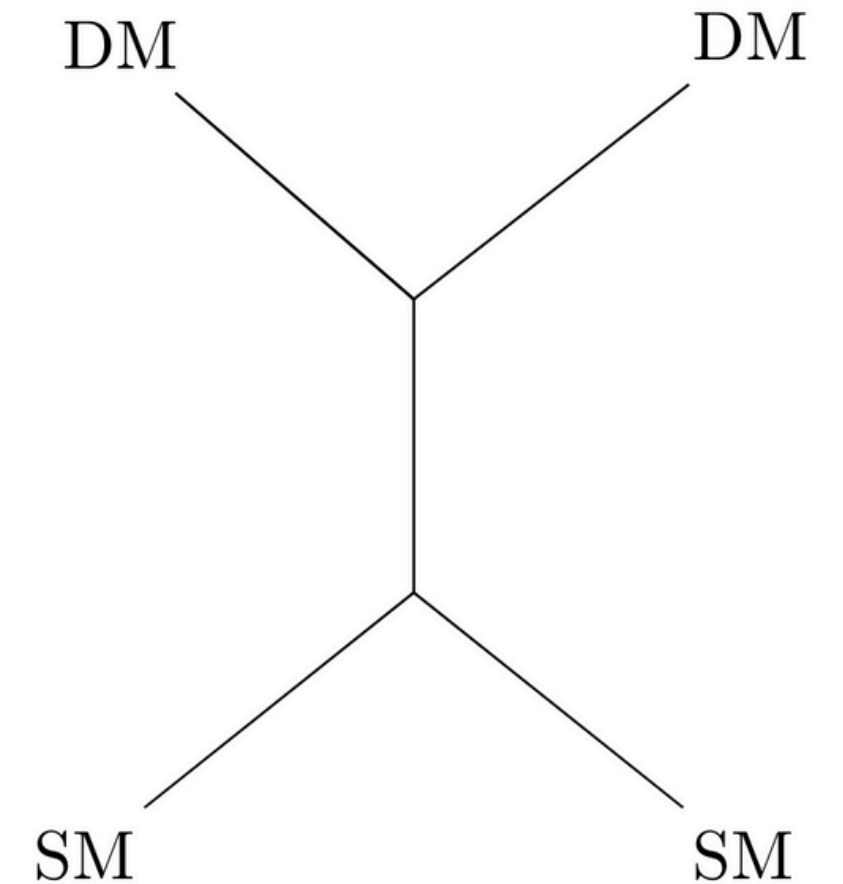
Difficulty:
kinetic decoupling

Kinetic Decoupling

$$\frac{1}{\Omega h^2} \propto \int \sigma_{\chi\chi \rightarrow f} = g_\chi g_{\text{SM}} \int \bar{\sigma}$$

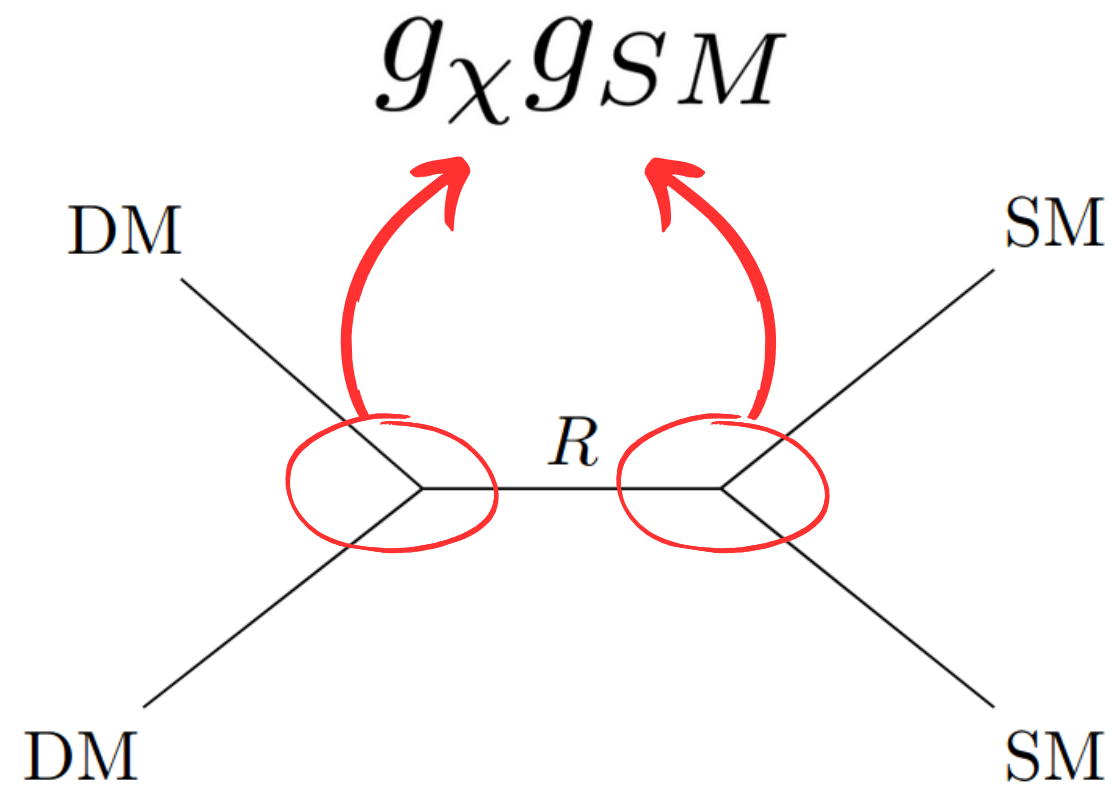


$$g_\chi g_{\text{SM}} \bar{\sigma}_{\text{scatt}}$$

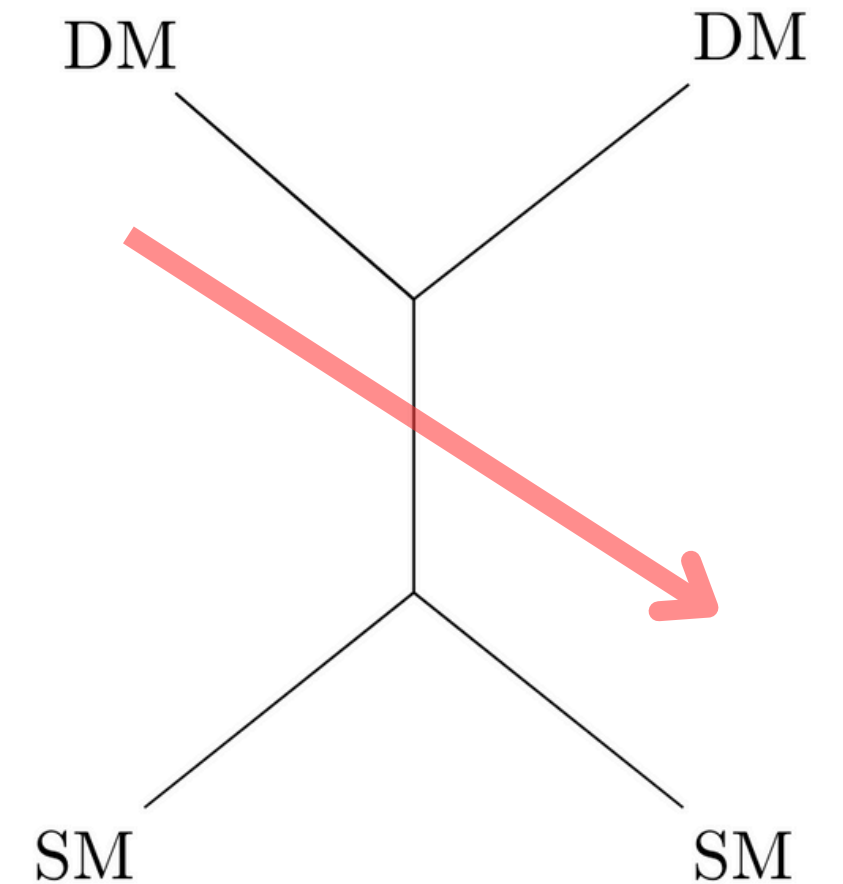


Kinetic Decoupling

$$\frac{1}{\Omega h^2} \propto \int \sigma_{\chi\chi \rightarrow f} = g_\chi g_{\text{SM}} \int \bar{\sigma}$$

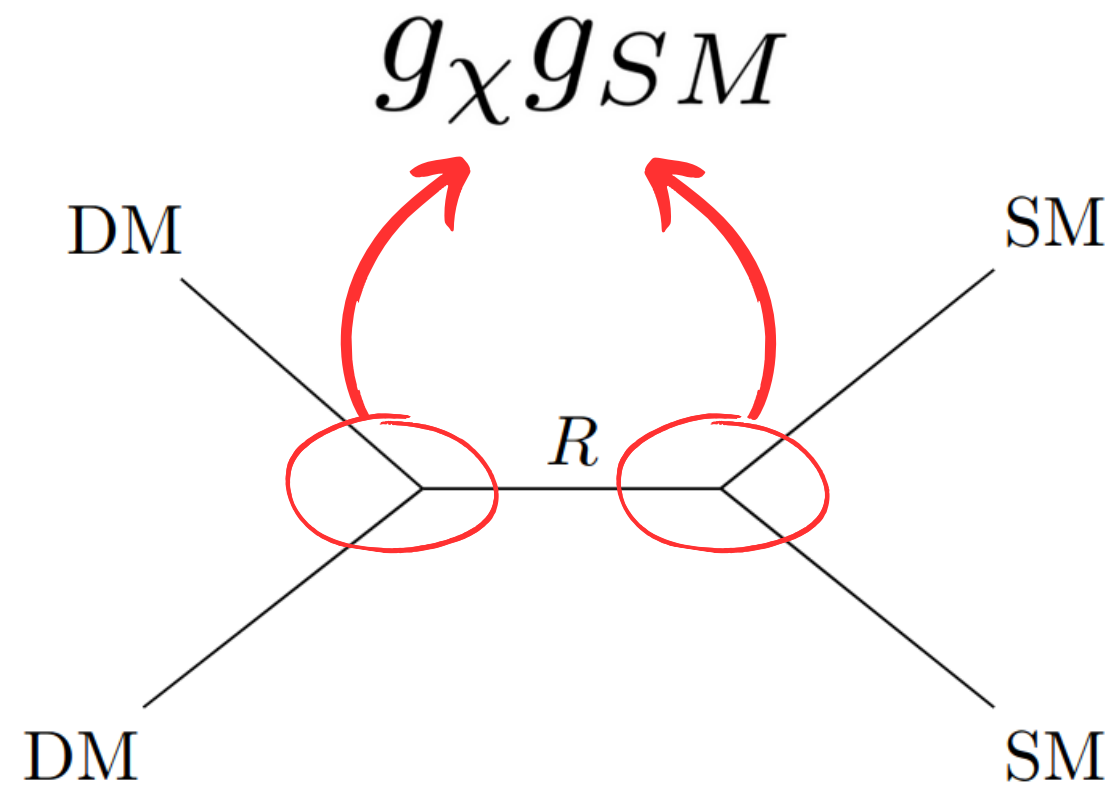


$$g_\chi g_{\text{SM}} \bar{\sigma}_{\text{scatt}}$$



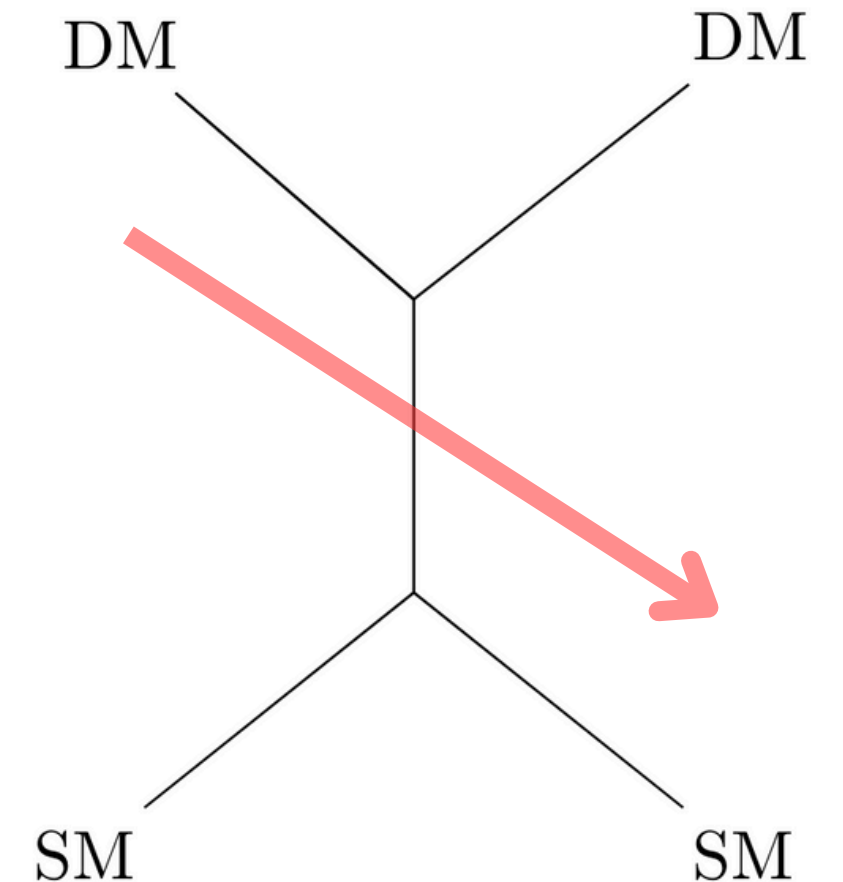
Kinetic Decoupling

$$\frac{1}{\Omega h^2} \propto \int \sigma_{\chi\chi \rightarrow f} = g_\chi g_{SM} \int \bar{\sigma}$$



$$g_\chi g_{SM} \bar{\sigma}_{\text{scatt}}$$

no longer efficient
exchange of energy



Kinetic decoupling

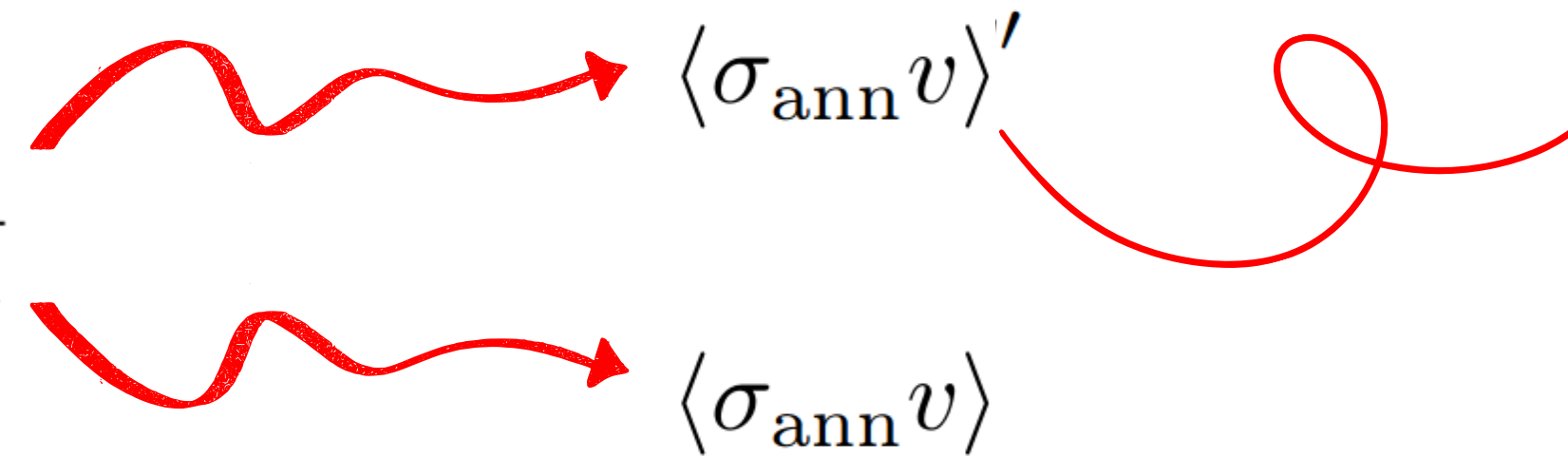
$$k_{\text{dec}} = \frac{\Omega_{\chi}}{\Omega_{\chi}^{\text{keq}}}$$

Hypothesis: enough DM self interaction

$$T' = \left(\frac{h_{\text{eff}}(T)}{h_{\text{eff}}(T_d)} \right)^{2/3} \frac{T^2}{T_d}$$

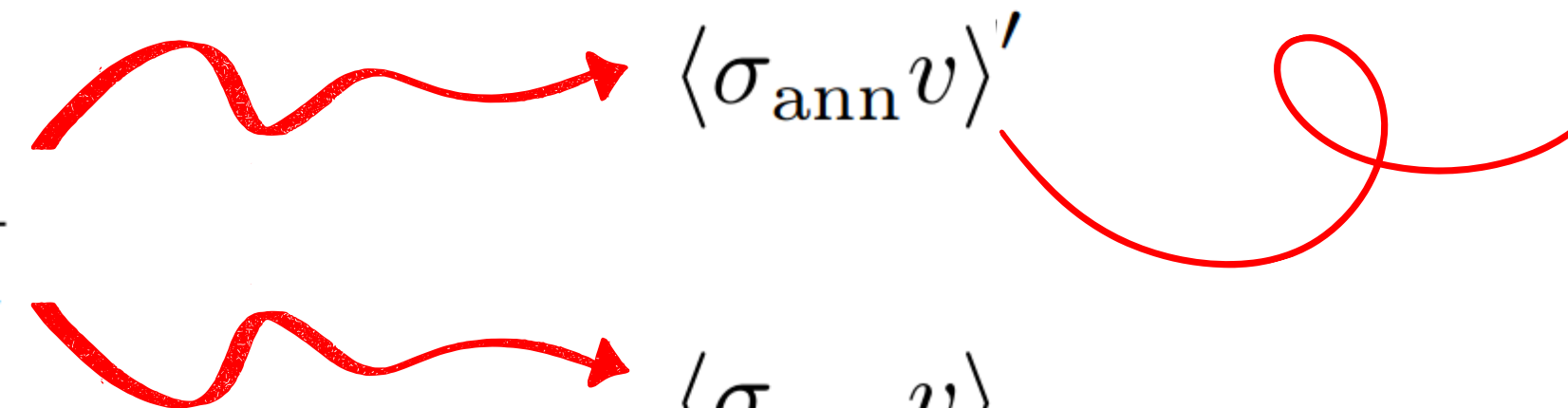
Kinetic decoupling

Hypothesis: enough DM self interaction


$$k_{\text{dec}} = \frac{\Omega_\chi}{\Omega_\chi^{\text{keq}}} \rightarrow \begin{cases} \langle \sigma_{\text{ann}} v \rangle' \\ \langle \sigma_{\text{ann}} v \rangle \end{cases} \rightarrow T' = \left(\frac{h_{\text{eff}}(T)}{h_{\text{eff}}(T_d)} \right)^{2/3} \frac{T^2}{T_d}$$


Kinetic decoupling

Hypothesis: enough DM self interaction

$$k_{\text{dec}} = \frac{\Omega_\chi}{\Omega_\chi^{\text{keq}}} \simeq \sqrt{\pi x_d \epsilon_R}$$

$$\langle \sigma_{\text{ann}} v \rangle'$$
$$\langle \sigma_{\text{ann}} v \rangle$$

$$T' = \left(\frac{h_{\text{eff}}(T)}{h_{\text{eff}}(T_d)} \right)^{2/3} \frac{T^2}{T_d}$$



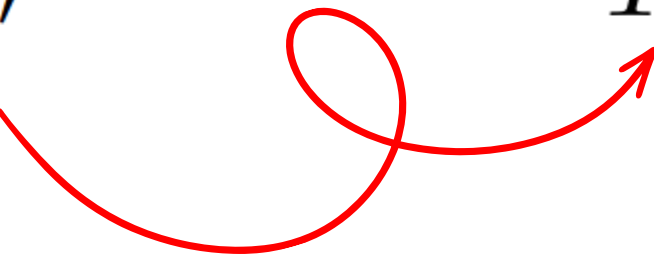

$$x_d = \frac{m_\chi}{T_d}$$


decoupling time

Kinetic decoupling

Hypothesis: enough DM self interaction

$$k_{\text{dec}} = \frac{\Omega_\chi}{\Omega_\chi^{\text{keq}}} \simeq \sqrt{\pi x_d \epsilon_R}$$

 $\langle \sigma_{\text{ann}} v \rangle'$
 $\langle \sigma_{\text{ann}} v \rangle$
 $T' = \left(\frac{h_{\text{eff}}(T)}{h_{\text{eff}}(T_d)} \right)^{2/3} \frac{T^2}{T_d}$
 $x_d = \frac{m_\chi}{T_d}$

To have a model-independent estimation of x_d :

decoupling time

$$\left(\frac{x_d}{x_f} \right)^2 \equiv r_{df}^2 = \frac{H(T_f)}{H(T_d)} = \frac{n_\chi \langle \sigma_{\text{ann}} v \rangle}{n_{\text{SM}} \langle \sigma_{\text{scatt}} v \rangle}$$

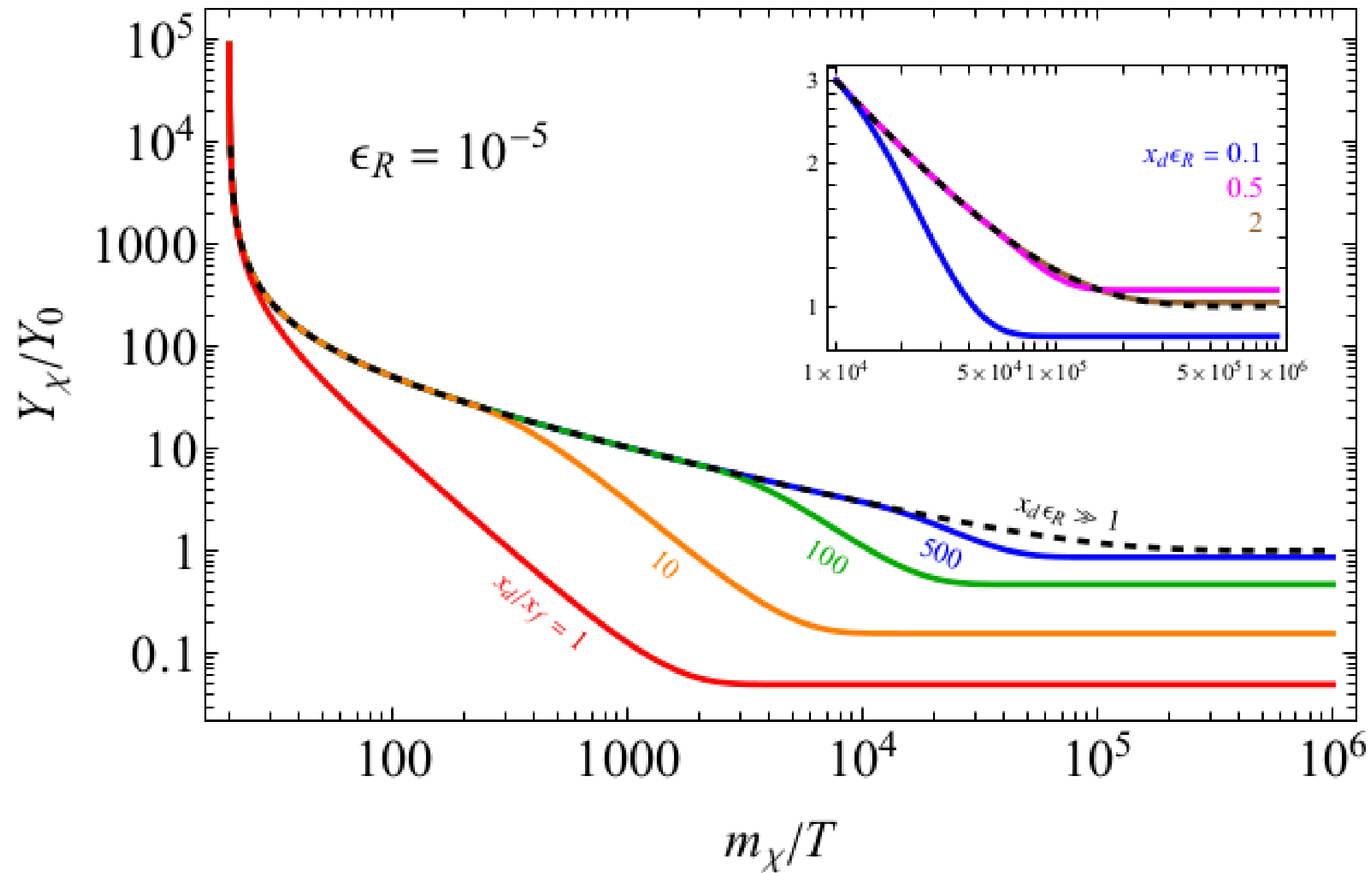
$$\Rightarrow r_{df} \simeq \begin{cases} \gamma_R / \gamma_R^c & \gamma_R > \gamma_R^c \\ 1 & \gamma_R \leq \gamma_R^c \end{cases}$$

$$\gamma_R^c \equiv x_f^{3/2} e^{-x_f} \approx 1.8 \times 10^{-7}$$

Belated Freeze out

x_f = freeze-out

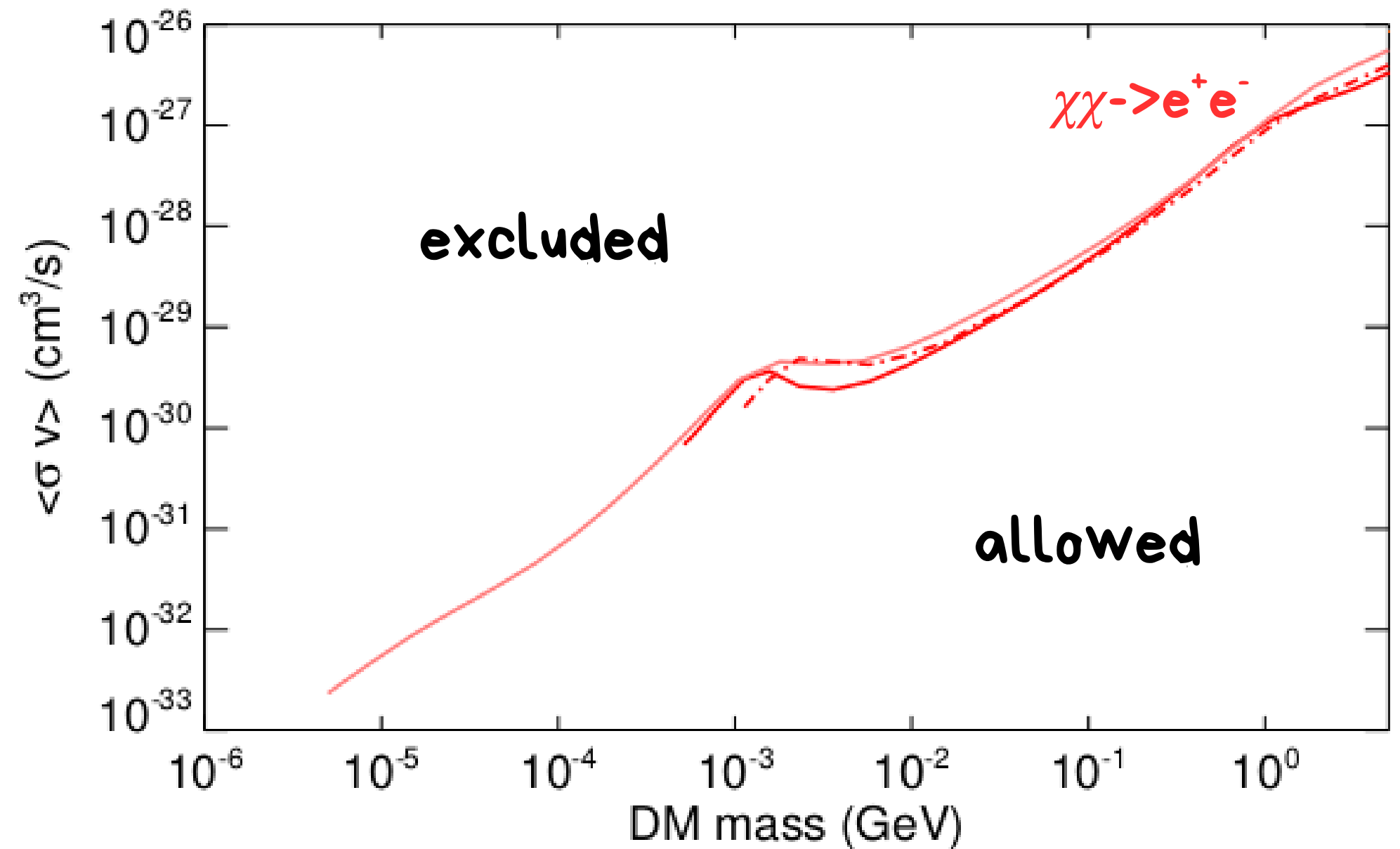
x_d = kinetic decoupling



CMB constraints

CMB constraints

Tracy R. Slatyer: Indirect Dark Matter Signatures in the Cosmic Dark Ages I.
Generalizing the Bound on s-wave Dark Matter Annihilation from Planck
arXiv:1506.03811



$$\langle\sigma v\rangle_{\epsilon\rightarrow 0}\approx 2.1\times 10^{-26}\text{ cm}^3/\text{s}\frac{N_{\chi}r_{df}^{1/2}\epsilon_R^{1/2}}{\bar{g}_{\star}^{1/2}f_{\chi}}\left[\frac{\gamma_R}{\gamma_R^2+\epsilon_R^2}\right]$$

CMB constraints

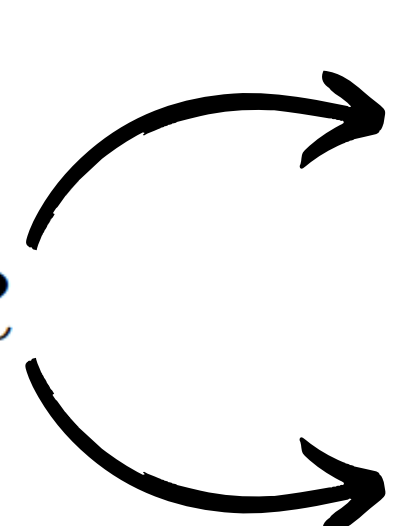
Relic density
imposed

$$\langle \sigma v \rangle_{\epsilon \rightarrow 0} \approx 2.1 \times 10^{-26} \text{ cm}^3/\text{s} \frac{N_\chi r_{df}^{1/2} \epsilon_R^{1/2}}{\bar{g}_*^{1/2} f_\chi} \left[\frac{\gamma_R}{\gamma_R^2 + \epsilon_R^2} \right]$$

different regimes:

large width: $\gamma_R \gg \epsilon_R$

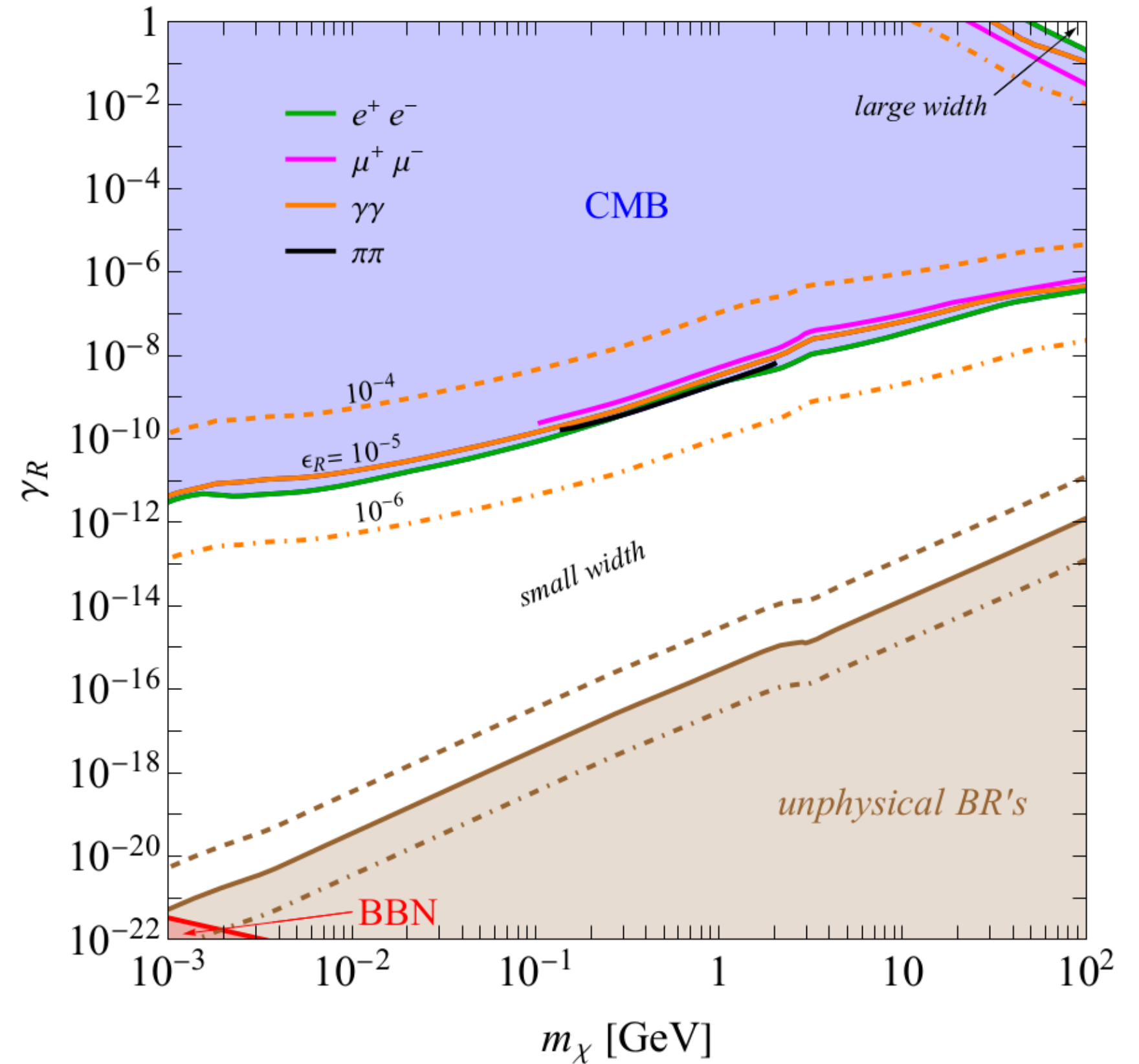
small width: $\gamma_R \ll \epsilon_R$


$$\gamma_R > \gamma_R^c$$
$$\gamma_R \leq \gamma_R^c$$

CMB constraints

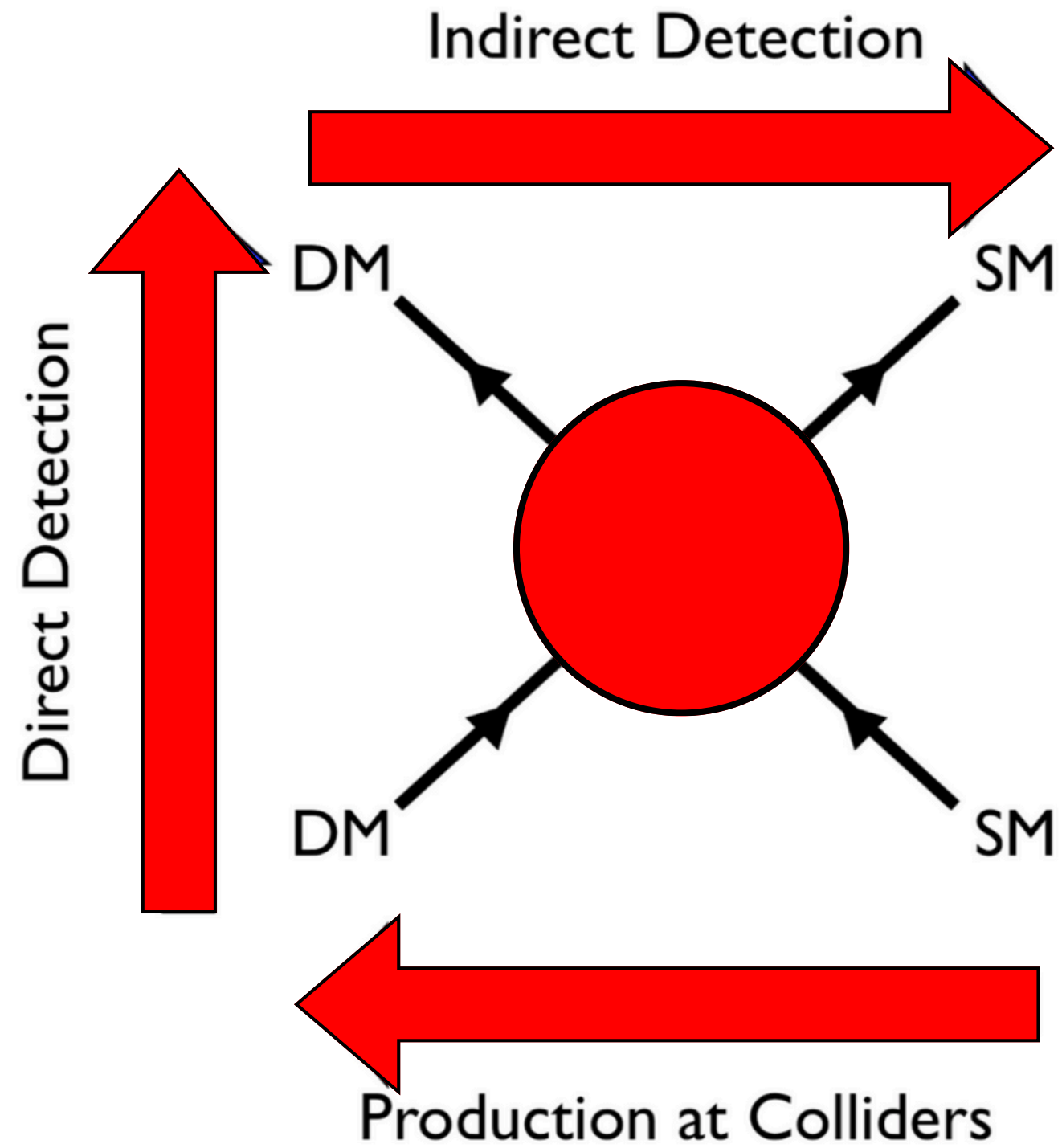
Extremely narrow states to
evade CMB constraints

$$10^{-16} \leq \gamma_R \leq 10^{-9} \text{ for } m_\chi = 1 \text{ GeV}$$

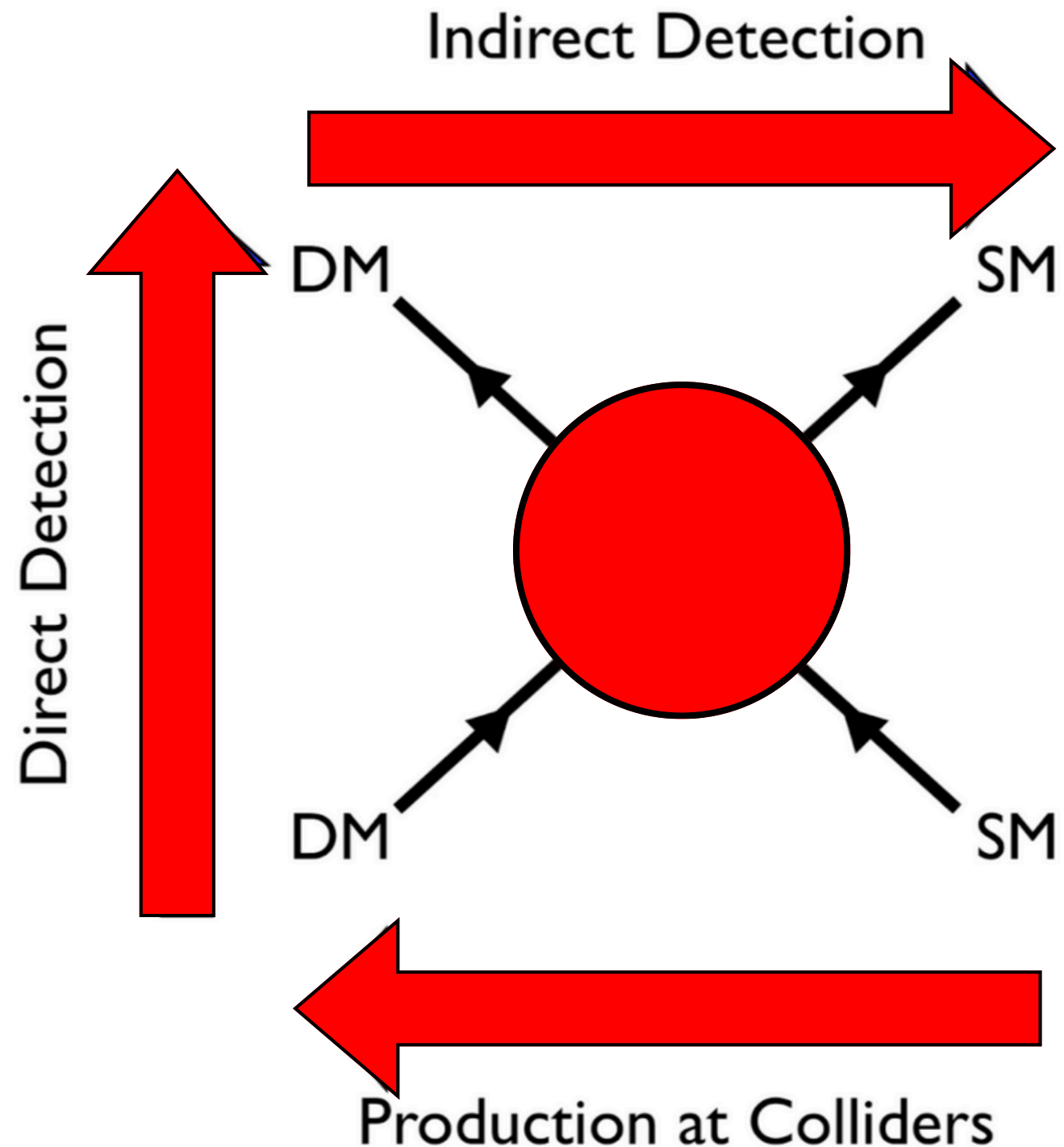


Possibility to detect DM
today ?

Indirect Detection



Indirect Detection



XMM-Newton: galactic halo (X-ray)

$v=220\text{km/s}$

MeerKAT: galaxy clusters (radio)

$v=1000\text{km/s}$

Fermi-LAT: dwarf galaxies (gamma-ray)

$v=2.5-10.7\text{km/s}$

Leo T: dwarf galaxy (gas cooling)

$v=7\text{km/s}$

Indirect Detection

XMM-Newton: galactic halo (X-ray)

$v=220\text{km/s}$

MeerKAT: galaxy clusters (radio)

$v=1000\text{km/s}$

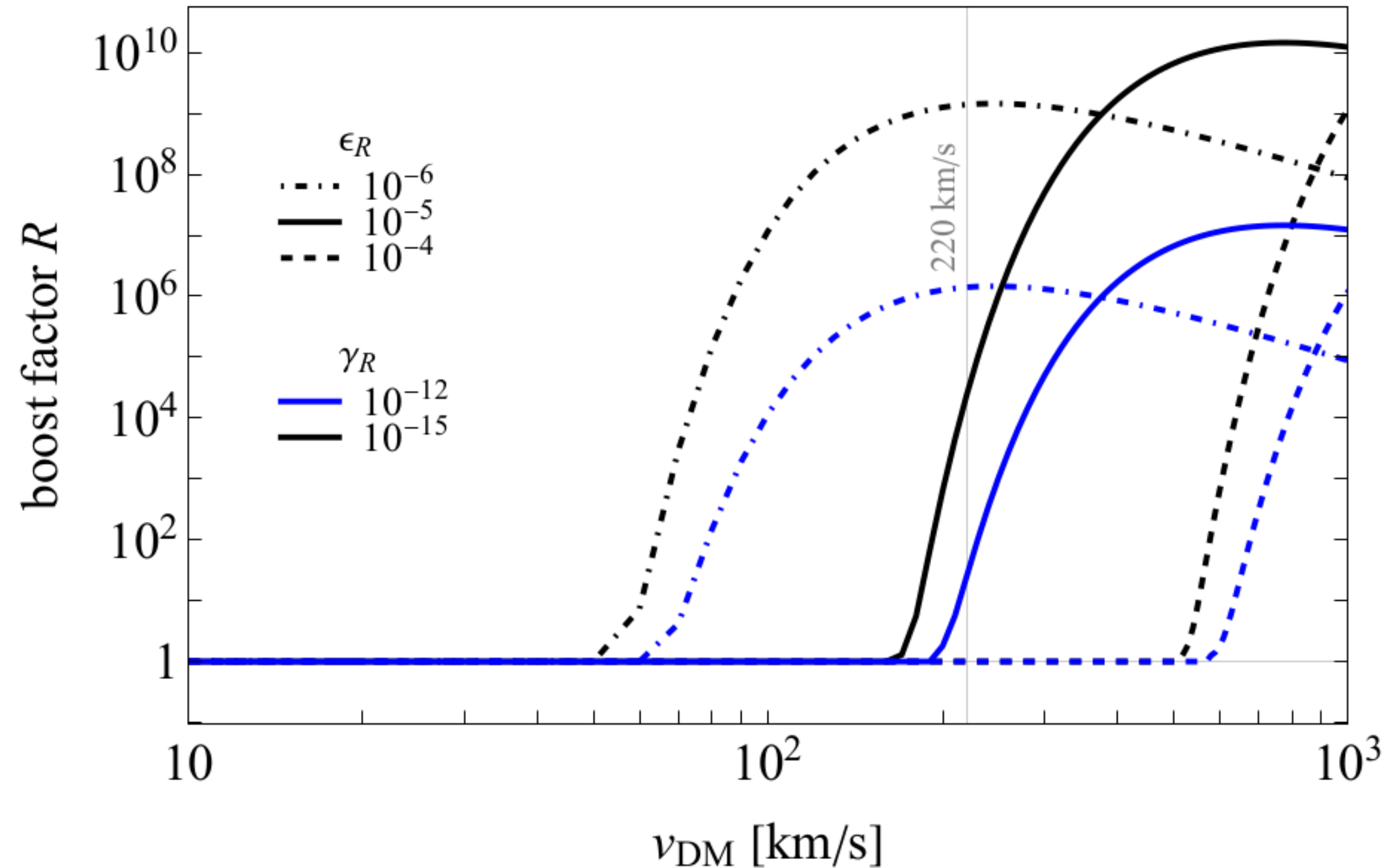
Fermi-LAT: dwarf galaxies
(gamma-ray)

$v=2.5-10.7\text{km/s}$

Leo T: dwarf galaxy (gas cooling)

$v=7\text{km/s}$

$$\langle\sigma v\rangle/\sigma v_0$$



Indirect Detection

Cirelli, Fornengo, Koechler, Pinetti, M. Roach: arXiv:2303.08854

Fermi-LAT collaboration: arXiv:1503.02641

Lavis, Sarkis, Beck, Knowles: arXiv:2308.08351

Wadekar, Wang: arXiv:2111.08025

XMM-Newton: galactic halo (X-ray)

$v=220\text{km/s}$

MeerKAT: galaxy clusters (radio)

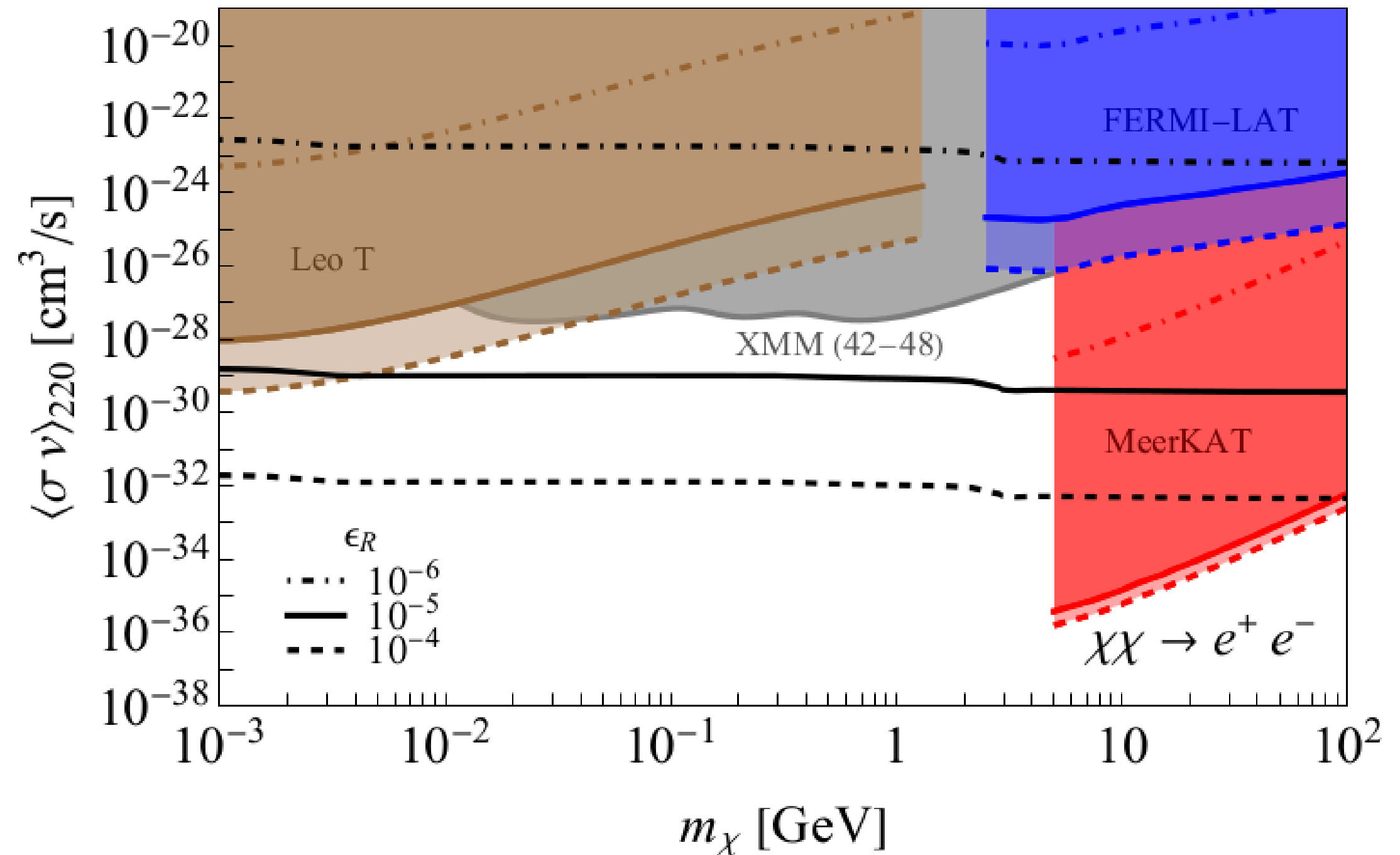
$v=1000\text{km/s}$

Fermi-LAT: dwarf galaxies
(gamma-ray)

$v=2.5-10.7\text{km/s}$

Leo T: dwarf galaxy (gas cooling)

$v=7\text{km/s}$



Conclusion

Thermal s-wave
Dark Matter

Conclusion

Thermal s-wave
Dark Matter

Relic density
constraints

CMB constraints

Conclusion

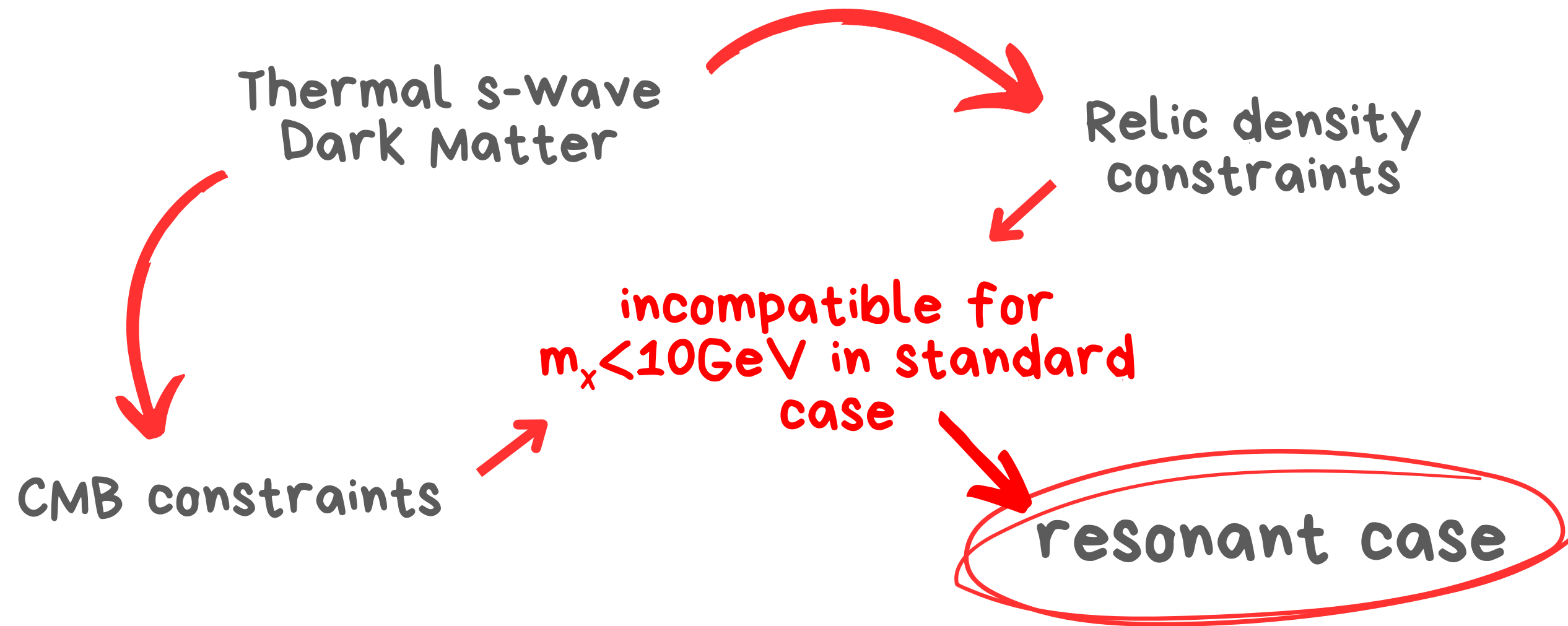
Thermal s-wave
Dark Matter

Relic density
constraints

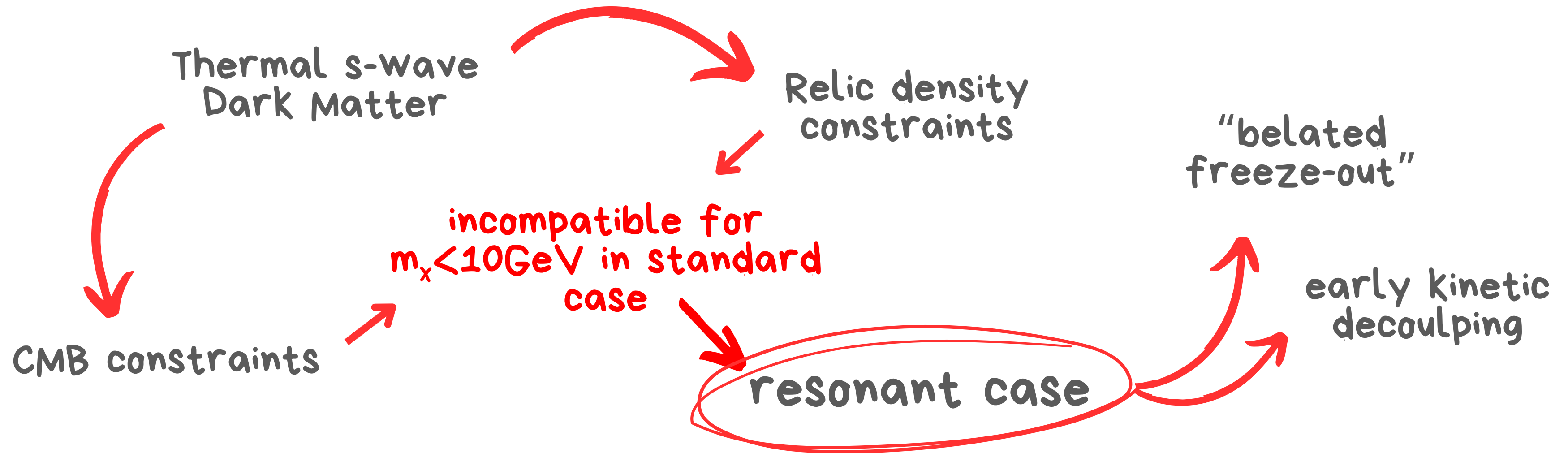
CMB constraints

incompatible for
 $m_x < 10\text{GeV}$ in standard
case

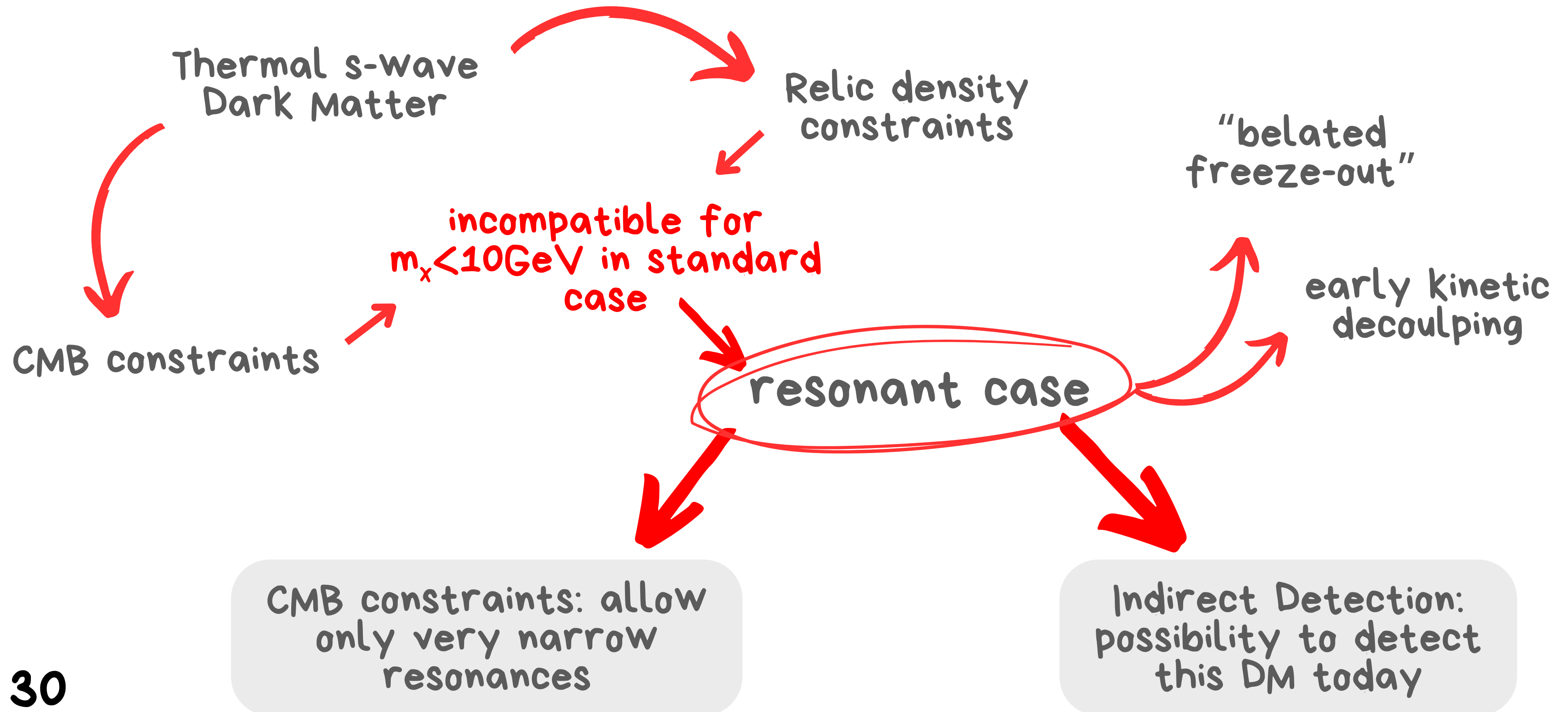
Conclusion



Conclusion



Conclusion



Thanks

II. RESONANT S-WAVE ANNIHILATION

Consider a DM particle χ of spin S_χ and mass m_χ , initially in thermal equilibrium with the SM plasma at early times ($T \gg m_\chi$). Near a resonance, its annihilation cross-section takes a generic BW form,

$$\sigma_{\chi\chi \rightarrow f} = \frac{4\pi\omega}{p^2} B_\chi B_f \frac{m_R^2 \Gamma_R^2}{(s - m_R^2)^2 + m_R^2 \Gamma_R^2}, \quad (1)$$

with $\omega \equiv (2J_R + 1)/(2S_\chi + 1)^2$, and $p \equiv \sqrt{s - 4m_\chi^2}/2$ is the DM center-of-mass momentum in terms of the total energy \sqrt{s} . The parameters J_R , m_R , and Γ_R denote the spin, mass, and total width of the resonance, respectively. The branching ratios are given by B_χ for resonance decay into DM pairs and $B_f = 1 - B_\chi$ for other final states. Since the (numerator of the) branching ratios in Eq. (1) are energy-dependent, and assuming s-wave dominance with negligible velocity-suppressed corrections, their product near the resonance follows,

$$B_\chi B_f \simeq \frac{p}{\bar{p}} \times \bar{B}_\chi \bar{B}_f, \quad (2)$$

where barred quantities denote their “on-shell” values at $\sqrt{s} = m_R$. Introducing the dimensionless parameters $\epsilon_R \equiv m_R^2/(4m_\chi^2) - 1$ and $\gamma_R \equiv m_R \Gamma_R/(4m_\chi^2)$, the annihilation cross-section times the lab-frame DM velocity reads [3],

$$\sigma v_{\text{lab}} = \frac{8\pi b_R (1 + \epsilon)^{1/2}}{m_\chi^2 (1 + 2\epsilon) \epsilon_R^{1/2}} \left[\frac{\gamma_R^2}{\gamma_R^2 + (\epsilon - \epsilon_R)^2} \right], \quad (3)$$

where $\epsilon \equiv (s - 4m_\chi^2)/(4m_\chi^2) \simeq v_{\text{lab}}^2/4$ is the squared relative DM velocity, and we define $b_R \equiv \omega \bar{B}_\chi (1 - \bar{B}_\chi) \leq \omega/4$.

III. BELATED FREEZE-OUT

We assume that DM particles were initially in chemical equilibrium with the SM in the early Universe and that the present relic density of DM has formed through the freeze-out mechanism. The Boltzmann equation governing the number density of DM is given by [1, 26, 27],

$$\dot{n}_\chi + 3H n_\chi = -\langle \sigma v \rangle (n_\chi^2 - n_{\chi \text{eq}}^2), \quad (4)$$

where H is the Hubble parameter, $n_{\chi \text{eq}}$ denotes the equilibrium DM density, and $\langle \sigma v \rangle$ is the thermally-averaged annihilation cross-section.

Following standard freeze-out calculations for resonant annihilation [3] which are briefly reviewed in appendix A, the contribution of χ to the energy budget of the Universe today is approximately,

$$\Omega_\chi h^2 \simeq 5.5 \times 10^{-13} N_\chi \frac{m_{\chi \text{GeV}}^2 \epsilon_R^{1/2}}{b_R \gamma_R \bar{g}_*^{1/2}}, \quad (5)$$

To evade strong CMB constraints while ensuring resonant enhancement at freeze-out, we impose $\epsilon_{\text{CMB}} \ll \epsilon_R \lesssim 1$. When $\epsilon_R \gg \epsilon_{\text{halo}} \sim 10^{-6}$, DM annihilation is only weakly enhanced in the Milky Way, limiting the indirect detection prospects. As we demonstrate below, existing searches already exclude resonant s-wave DM with $\epsilon_R \lesssim 10^{-6}$. We thus focus on ϵ_R in the range $10^{-4} - 10^{-6}$ in the following.

Such a fine-tuned mass coincidence between DM and the mediator is not natural in the 't Hooft sense within minimal models. A notable exception arises in Kaluza-Klein DM models [23] based on large extra dimensions [24, 25], where $m_R = 2m_\chi$ can be achieved at tree-level. Nevertheless, this scenario remains phenomenologically compelling, representing one of the last viable scenarios for thermal s-wave DM below $m_\chi \sim 10$ GeV. A key feature of these resonances is their significant impact on freeze-out dynamics, delaying it well beyond the point of chemical decoupling from the thermal bath.

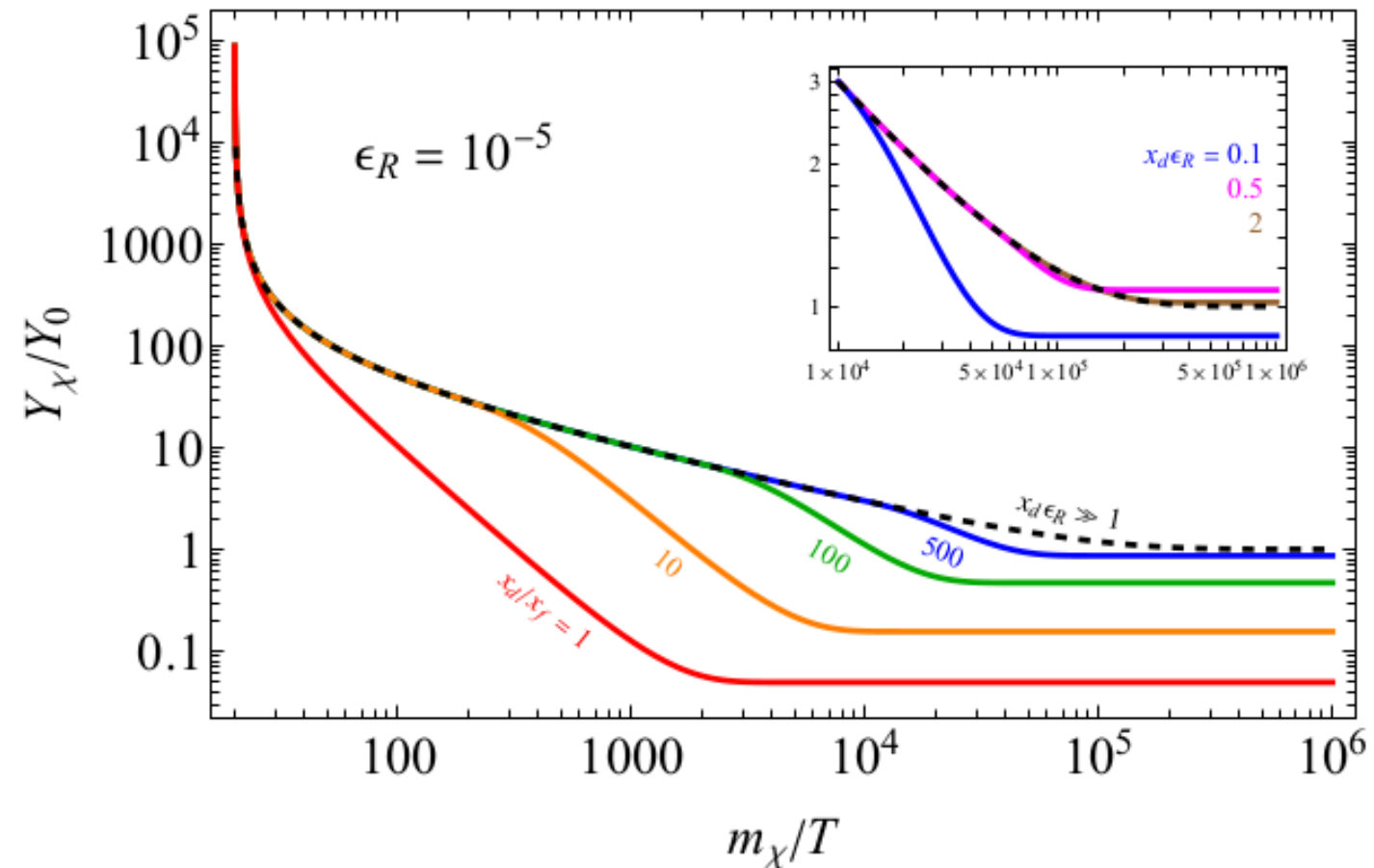


FIG. 1. DM abundance Y_χ as function of time, parameterized by $x = m_\chi/T$, after chemical decoupling at $x_f = 20$ in the belated freeze-out scenario for $\epsilon_R = 10^{-5}$. The dashed line assumes kinetic equilibrium ($x_d \epsilon_R \gg 1$), while the red, orange, green and blue curves represent the suppression due to kinetic decoupling at $x_d/x_f = 1, 10, 100$, and 500 , respectively. The inset highlights the mild enhancement of the abundance for very late decoupling at $x_d \epsilon_R = 1/2$ (magenta) and 2 (brown). Abundances are shown in units of the kinetic equilibrium value at $x \rightarrow \infty$, denoted as Y_0 .

where $N_\chi = 1$ ($N_\chi = 2$) when χ and $\bar{\chi}$ are (not) identical particles, $m_{\chi\text{GeV}}$ is the DM mass in GeV, and $\bar{g}_\star^{1/2}$ is the effective number of degree-of-freedom of the SM plasma at the time of chemical decoupling. This expression assumes that DM exchanges energy with the SM sufficiently fast to maintain a thermal distribution throughout freeze-out. However, for highly effective resonant annihilation, this kinetic-equilibrium condition is typically not met [17], as the DM-SM scattering cross-section does not benefit from the resonance and is suppressed by small couplings. In such scenarios, the Boltzmann equation must be solved directly for the DM momentum distribution rather than the number density. This is a challenging numerical task [18], requiring detailed modeling to relate the scattering and annihilation cross-sections. To keep the discussion general, we parameterize corrections

to eq. (5) from early kinetic decoupling with a model-dependent normalization factor k_{dec} . Thus, we write,

$$b_R \gamma_R \epsilon_R^{-1/2} = 4.6 \times 10^{-12} k_{\text{dec}} N_\chi \frac{m_{\chi\text{GeV}}^2}{\bar{g}_\star^{1/2} f_\chi}, \quad (6)$$

where $f_\chi \equiv \Omega_\chi/\Omega_{\text{DM}}$ is the fraction of the total amount of DM observed, with $\Omega_{\text{DM}} h^2 \approx 0.12$, that is in the form of χ (and eventually $\bar{\chi}$) particles. We will show in section IV that for $\epsilon_R \ll 1$, k_{dec} is expected to be much smaller than unity, meaning the relic density is strongly suppressed, with the approximate scaling $k_{\text{dec}} \propto \sqrt{\epsilon_R}$.

Figure 1 shows that for $\epsilon_R \ll 1$, the abundance of χ continues to evolve long after chemical decoupling, resulting in a belated freeze-out regime. Although the annihilation rate has fallen below the Hubble expansion rate, the annihilation cross-section continues to grow at lower temperatures [5]. As DM particles cool, the peak of their velocity distribution aligns more closely with the resonance peak. Consequently, the DM yield slowly fades out, scaling approximately as $x^{-1/2}$ where $x \equiv m_\chi/T$, until $x \sim \epsilon_R^{-1}$, at which point DM particles are too cold to satisfy the resonance condition. While this description remains qualitatively correct, it is significantly modified by kinetic decoupling, which, as we argue below, likely occurs in the course of this evolution.

The right-hand side of the Boltzmann equation in eq. (4) is modified to,

$$\begin{aligned} \dot{n}_\chi + 3Hn_\chi &= -\langle\sigma v\rangle' n_\chi^2 + \langle\sigma v\rangle n_{\chi\text{eq}}^2 \\ &= -\langle\sigma v\rangle [\beta(\xi)n_\chi^2 - n_{\chi\text{eq}}^2] , \end{aligned} \quad (9)$$

where $\langle\sigma v\rangle'$ is obtained by taking $T \rightarrow T'$ in $\langle\sigma v\rangle$, and the second line assumes resonant annihilation, with,

$$\beta(\xi) \equiv \xi^{-3/2} e^{-x\epsilon_R(\xi^{-1}-1)} . \quad (10)$$

We show in appendix B that solving eq. (9) approximately yields,

$$k_{\text{dec}} \simeq \left[\text{erf}(y_d) - \text{erf}(y_f) + \frac{e^{-y_d^2}}{2\sqrt{\pi}y_d} \right]^{-1} , \quad (11)$$

where $y \equiv \sqrt{x\epsilon_R}$, and erf is the error function. The first two terms (last term) in the square brackets correspond to DM annihilation before (after) kinetic decoupling. In the regime $x_d\epsilon_R \ll 1$, the last term dominates, yielding a suppression of the relic density relative to the usual result without kinetic decoupling,

$$k_{\text{dec}} \simeq 2\sqrt{\pi x_d\epsilon_R} \ll 1 . \quad (12)$$

IV. KINETIC DECOUPLING

Resonant annihilation typically requires much smaller coupling values to achieve the correct DM relic density. This generally leads to kinetic decoupling of DM during the freeze-out process. Below, we estimate the kinetic-decoupling correction parameter,

$$k_{\text{dec}} \equiv \frac{\Omega_\chi}{\Omega_\chi^{\text{keq}}}, \quad (7)$$

where Ω_χ^{keq} denotes the abundance obtained from eq. (5) under the assumption of kinetic equilibrium.

We assume the DM particles are in sufficiently fast self-interactions, allowing them to form a dark equilibrium at temperature $T' \leq T$ after decoupling at $T = T_d$. For $T \geq T_d$, $T' = T$, while for $T < T_d$, the DM temperature evolves with time according to,

$$T'(T < T_d) \equiv \xi(T)T, \quad \xi(T) = \left[\frac{h_{\text{eff}}(T)}{h_{\text{eff}}(T_d)} \right]^{2/3} \frac{T}{T_d}. \quad (8)$$

The linear scaling with T follows from the fact that DM is non-relativistic at decoupling, while the prefactor captures the subsequent reheating of the SM plasma due to the decoupling of SM species; h_{eff} denotes the number of degrees of freedom of the entropy density.

Once kinetic decoupling occurs, DM particles, being non-relativistic, cool more rapidly than the thermal bath, with $T' \propto T^2$. This causes the resonance condition to be satisfied earlier, maximizing the annihilation cross-section when the Universe's entropy density is still

high and DM particles are less diluted. As a result, the DM yield decreases more rapidly, scaling approximately as x^{-2} . This effect weakens the later the kinetic decoupling occurs. In the opposite limit, $x_d \epsilon_R \gg 1$, the relic density remains unchanged, as expected, since the DM yield stops evolving after $x \sim \mathcal{O}(\epsilon_R^{-1})$. Interestingly, k_{dec} in eq. (12) reaches a maximum at finite $x_d = (2\epsilon_R)^{-1}$. This implies a window of enhanced relic density, though only by a modest factor of $\mathcal{O}(10\%)$ at most, with a mild ϵ_R -dependence from the $\text{erf}(y_f)$ term. The reason for this is that, at temperatures where the peak of the DM velocity distribution has moved past the resonance, annihilation becomes less efficient. This is because the distribution shifts away from the resonance more rapidly than in kinetic equilibrium, diminishing the overlap of the distribution's tail at later times. When decoupling occurs for $x_d \sim \epsilon_R^{-1}$, where the enhancement discussed earlier has largely diminished, this effect becomes dominant, leading to a slightly higher DM abundance. Figure 1 shows the evolution of Y_χ with time for various kinetic decoupling temperatures.

where $\gamma_R^c \equiv x_f^{3/2} e^{-x_f} \approx 1.8 \times 10^{-7}$. Equation (13) may change in models where additional scattering processes, distinct from the crossing-symmetric counterparts of the annihilation processes, also contribute efficiently to maintain kinetic equilibrium. These processes could extend the period of equilibrium beyond the estimate in eq. (13) and potentially modify the dependence on resonance parameters. In the following, we disregard such processes and assume that eq. (13) remains valid.

Kinetic equilibrium is maintained at least until chemical decoupling occurs at $x_f \approx 20$ thanks to the annihilation process itself [11]. Whether kinetic equilibrium persists to lower temperatures depends on the efficiency of scattering processes. While model-dependent, the generic properties of such processes can still be assessed. After chemical decoupling, the scattering rate $n_{\text{SM}}\langle\sigma_{\text{scat.}}v\rangle$ typically remains faster than Hubble expansion because the SM number density n_{SM} is not Boltzmann suppressed, ensuring kinetic equilibrium until well beyond freeze-out in models where the scattering and annihilation cross-sections are comparable. Here, however, unlike annihilation, scattering is not resonantly enhanced and is expected to be suppressed by a factor of $\mathcal{O}(\gamma_R)$ relative to annihilation. For sufficiently small resonance widths, the scattering rate is generically subdominant to the annihilation rate, so kinetic decoupling occurs immediately after chemical decoupling. For larger width values, scattering is less suppressed relative to annihilation, and kinetic decoupling is delayed well after T_f . We show in appendix B that $r_{df} \equiv T_f/T_d$ is, approximately,

$$r_{df} \simeq \begin{cases} \gamma_R/\gamma_R^c & \gamma_R > \gamma_R^c \\ 1 & \gamma_R \leq \gamma_R^c \end{cases}, \quad (13)$$

where we include in the second equality the effect of kinetic decoupling using eq. (12) in eq. (5). The CMB bound can also be evaded if $\epsilon_R \ll \epsilon_{\text{CMB}}$, but since $\epsilon_{\text{CMB}} \lesssim 10^{-11}$ for GeV-scale DM, this would require extreme fine-tuning of dark sector masses, so we do not consider this scenario further.

An upper bound $\langle\sigma v\rangle_{\text{CMB}}$ from CMB anisotropies constrains the resonance width, yielding two possible regimes based on γ_R/ϵ_R (see appendix D): (i) a *large-width* regime with $\gamma_R \gg \epsilon_R$, and (ii) a *small-width* regime with $\gamma_R \ll \epsilon_R$. In the large-width regime, CMB imposes a lower bound on the resonance width,

$$\gamma_R \gtrsim 27 X^2 \left[\frac{\epsilon_R}{10^{-5}} \right], \quad (15)$$

with

$$X \equiv \frac{N_\chi \langle\sigma v\rangle_{\text{th}}}{\bar{g}_\star^{1/2} f_\chi \langle\sigma v\rangle_{\text{CMB}}}, \quad (16)$$

which is deeply in the non-perturbative regime unless the CMB bound is significantly weaker than the typical thermal cross section $\langle\sigma v\rangle_{\text{th}}$. Conversely, in the small-width regime, CMB implies a rather strong upper bound on the width,

$$\gamma_R \lesssim \frac{4.5 \times 10^{-8}}{X} \left[\frac{\epsilon_R}{10^{-5}} \right]^{3/2}, \quad (17)$$

V. CMB CONSTRAINTS

DM annihilation during recombination injects energy that heats and reionizes the photon-baryon plasma, affecting the CMB temperature and polarization fluctuations [28]. Observations from the Planck satellite place stringent constraints on DM annihilation at that time [29]. In particular, for annihilation into electron pairs, CMB data exclude cross-sections as large as $\langle\sigma v\rangle_{\text{th}} = 3 \times 10^{-26} \text{ cm}^3/\text{s}$, for DM below $m_\chi \simeq 10 \text{ GeV}$ [10]. This typically rules out standard freeze-out via s-wave annihilation in this channel. However, we show that resonant annihilation can evade these bounds and determine the resonance parameters required for various final states, including electrons, muons, pions, and photons.

At recombination, DM particles are typically very cold, with $\epsilon_{\text{CMB}} \ll 1$ when the Universe's temperature is $T_{\text{CMB}} \approx 2.6 \text{ eV}$. If $\epsilon_R \gg \epsilon_{\text{CMB}}$, the annihilation cross-section at that time is non-resonant and well approximated by the zero-velocity limit ($\epsilon \rightarrow 0$) of eq. (3), typically valid for $\epsilon_R \sim 10^{-5}$ (see appendix C). This gives,

$$\begin{aligned} \langle\sigma v\rangle_{\text{CMB}} &= \frac{8\pi b_R}{m_\chi^2 \epsilon_R^{1/2} (\gamma_R^2 + \epsilon_R^2)} \\ &\approx 2.1 \times 10^{-26} \text{ cm}^3/\text{s} \frac{N_\chi r_{df}^{1/2} \epsilon_R^{1/2}}{\bar{g}_\star^{1/2} f_\chi} \left[\frac{\gamma_R}{\gamma_R^2 + \epsilon_R^2} \right], \end{aligned} \quad (14)$$

provided $\gamma_R < \gamma_R^c$, or

$$\gamma_R \lesssim \frac{7.2 \times 10^{-8}}{X^{2/3}} \left[\frac{\epsilon_R}{10^{-5}} \right], \quad (18)$$

when $\gamma_R > \gamma_R^c$, which suggests very weak resonance's couplings to DM and SM particles in this regime.

Figure 2 shows the allowed resonance widths for DM annihilation into electrons, muons, pions, and photons as a function of the DM mass and for different values of ϵ_R . We use `micrOMEGAs` to derive the CMB constraint for the electron, muon, photon and pion channels, following the approach outlined in [10] and accounting for the most recent Planck data [29]. The pion bound assumes annihilation into both $\pi^0\pi^0$ and $\pi^+\pi^-$ final states, with cross-sections related by isospin symmetry, though the neutral pion contribution largely dominates. Furthermore, for the interested reader, we provide CMB bounds for several individual channels in appendix E.

The small-width regime is bounded from below by the condition $\gamma_R \gtrsim 3.3 \times 10^{-25}/m_\chi \text{ GeV}$ that the resonance lifetime does not exceed one second so that it has disappeared from the Universe before the onset of Big Bang nucleosynthesis (BBN), and by the condition $b_R < \omega/4$ corresponding to physically relevant resonance BRs. For electrons with assuming $\epsilon_R = 10^{-5}$, the CMB constraint excludes the large-width regime up to $m_\chi \approx 40 \text{ GeV}$. In the small-width regime, it forces the resonance to be extremely narrow, as small as $\sim 10^{-12}$ of its mass for $m_\chi \approx 1 \text{ MeV}$.

For DM below 10 MeV annihilating into electrons and photons, constraints from N_{eff} (not shown in fig. 2) may also be relevant (see, *e.g.*, [30–32]). However, these bounds are model-dependent, as they vary with the DM spin and can be significantly relaxed, in some cases down to $m_\chi \simeq 1$ MeV, if additional couplings to neutrinos are present [30].

VI. INDIRECT DETECTION SIGNALS

We now examine signals of DM annihilation in the present Universe, focusing on the galactic halo, dwarf galaxies, and galactic clusters. For resonant s-wave annihilation, the predicted cross-section depends strongly on the DM velocity. We assume that DM particles have virialized within these astrophysical systems, following a Maxwell-Boltzmann distribution with a dispersion velocity v_{DM} . In the small-width regime, and under the relic density constraint from eq. (6), the velocity-averaged annihilation cross-section is given by,

$$\begin{aligned} \langle \sigma v \rangle \simeq & 1.9 \times 10^{-21} \text{ cm}^3/\text{s} \frac{N_\chi}{\bar{g}_\star^{1/2} f_\chi} \left(\frac{v_\odot}{v_{\text{DM}}} \right)^3 \left[\frac{\epsilon_R}{10^{-5}} \right] \\ & \times \exp \left[-18.6 \left(\frac{v_\odot}{v_{\text{DM}}} \right)^2 \left[\frac{\epsilon_R}{10^{-5}} \right] \right], \end{aligned} \quad (19)$$

where $v_\odot \equiv 220$ km/s is the typical velocity dispersion in the Milky Way halo at a distance of ~ 10 kpc from the Galactic center [33, 34]. Notably, $\langle \sigma v \rangle$ in eq. (19) is independent on the resonance width γ_R and only weakly depends on the DM mass via the number of relativistic degrees of freedom present in the early Universe at the time of DM chemical decoupling \bar{g}_\star . In astrophysical environments where v_{DM} is much smaller than v_\odot , such as dwarf galaxies, the cross-section is no longer resonantly enhanced and instead approaches the zero-velocity limit,

$$\begin{aligned} \sigma v_0 \equiv \sigma v_{\epsilon \rightarrow 0} \simeq & 6.7 \times 10^{-31} \text{ cm}^3/\text{s} \frac{N_\chi}{\bar{g}_\star^{1/2} f_\chi} \\ & \times \left[\frac{\gamma_R}{10^{-12}} \right] \left[\frac{\epsilon_R}{10^{-5}} \right]^{-3/2}, \end{aligned} \quad (20)$$

which is the same cross-section relevant during recombination. Additionally, σv_0 depends weakly on m_χ through \bar{g}_\star .

Figure 3 illustrates the boost factor $R \equiv \langle \sigma v \rangle / \sigma v_0$ due to BW effects as a function of the DM dispersion velocity, for different values of ϵ_R and γ_R , highlighting

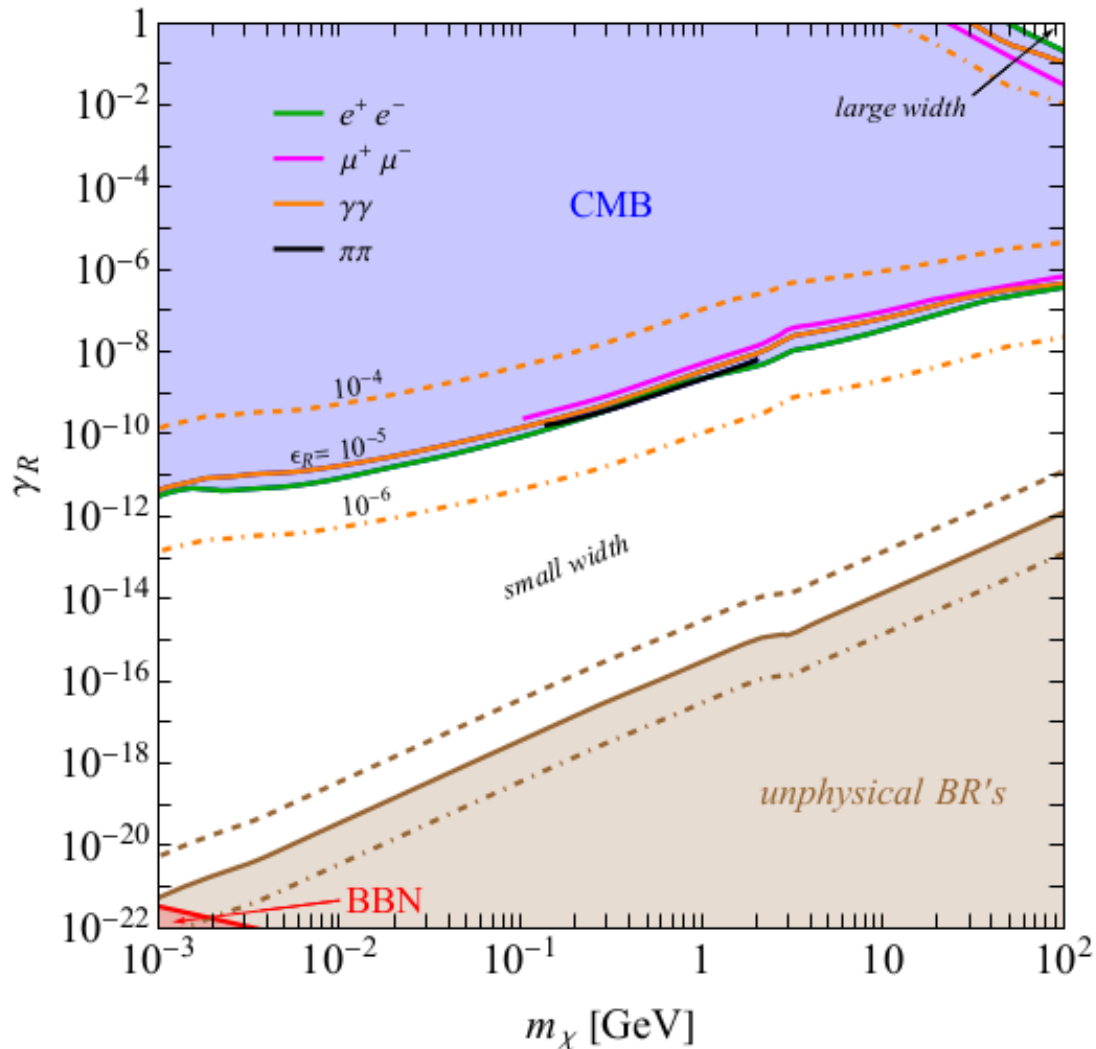


FIG. 2. Resonance width γ_R as function of the DM mass m_χ . The blue-shaded area is excluded by CMB observations with different boundaries representing annihilation to electrons (green), muons (magenta), photons (orange) and pions (black), assuming $\epsilon_R = 10^{-5}$. The pion bound assumes annihilation into both $\pi^0\pi^0$ and $\pi^+\pi^-$ channels, assuming isospin symmetry. The red region corresponds to resonance lifetime exceeding one second, potentially affecting BBN predictions. In the brown-shaded region the resonance branching ratios are not physical ($b_R > \omega/4$, assuming $J_R = 1, S_\chi = 0$). Dashed and dot-dashed lines represent results for resonances with $\epsilon_R = 10^{-4}$ and 10^{-6} , respectively, showing only photons for the CMB exclusion. The allowed regions above and below the CMB exclusion correspond to the large-width and small-width regimes, respectively, as defined in the text.

A variety of indirect detection (ID) experiments search for the products of DM annihilation in different astrophysical environments. These constraints typically assume a velocity-independent s-wave annihilation cross-section. However, near a resonance, the cross-section exhibits strong velocity dependence, necessitating a recasting of experimental limits.

The Fermi-LAT telescope observes gamma-ray emissions from dwarf galaxies [21], where typical DM velocity dispersions range from 2.5 km/s to 10.7 km/s [35]. At these low velocities, DM annihilation occurs far from the resonance, justifying the zero-velocity approximation $\langle\sigma v\rangle_{\text{Fermi-LAT}} \approx \sigma v_0$. Similarly, for constraints based on gas cooling observations of the **Leo T** dwarf galaxy [36], where the DM velocity is estimated to be around 7 km/s [37, 38].

Powerful constraints can be extracted from X-ray data of XMM-Newton [20], which observes the entire galaxy and derives limits from concentric rings. We use the constraint from the $42^\circ - 48^\circ$ latitude region, which provides to the strongest limits away from the galactic center (GC). In this region, the dominant contribution to DM annihilation comes from DM particles with a velocity v_\odot . The X-ray constraints are subject to large uncertainties; here, we adopt the central value from [20].

We also incorporated radio constraints from the MeerKAT telescope, which detects synchrotron emissions from galaxy clusters and dwarf galaxies using radio interferometry [39, 40]. We focus on constraints from galaxy clusters, which have fewer astrophysical uncertainties and provide more robust bounds [22]. Using

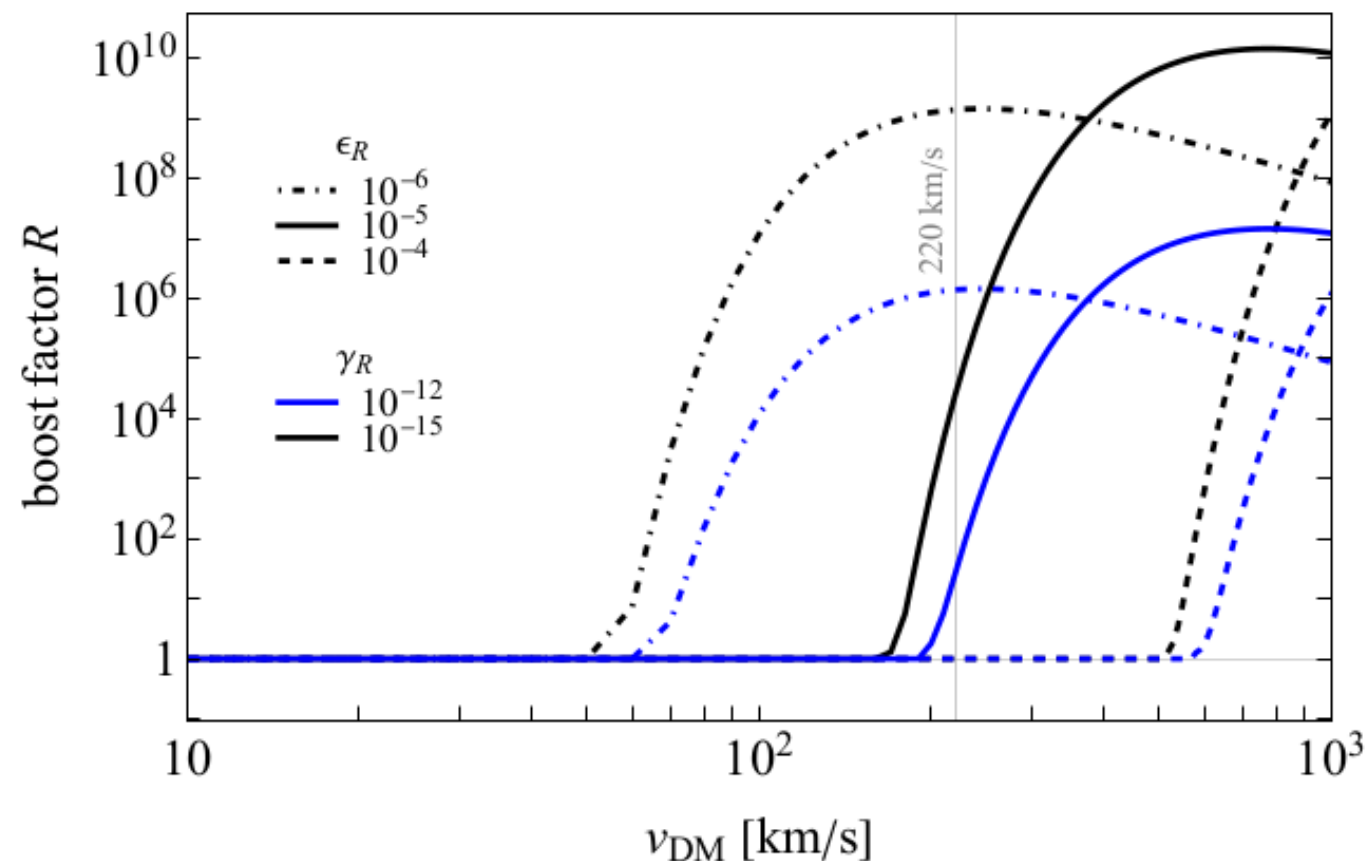


FIG. 3. Boost factor $R \equiv \langle \sigma v \rangle / \sigma v_0$ of the DM annihilation cross-section as function of the DM dispersion velocity v_{DM} , relative to its zero-velocity counterpart, *i.e.*, the cross-section relevant during recombination. Dashed, solid and dot-dashed lines correspond to $\epsilon_R = 10^{-4}$, 10^{-5} and 10^{-6} , respectively, with fixed $\gamma_R = 10^{-12}$ (blue) and 10^{-15} (black). The vertical gray line marks the typical DM velocity dispersion $v_\odot = 220$ km/s in the Milky Way’s halo, excluding the Galactic center [33, 34].

the linear dependence of R on γ_R .

DarkMatters [41], we computed the radio flux from DM annihilation into electrons and muons and compared them to MeerKAT’s L-band sensitivity [42]. The typical DM velocity in these clusters is ~ 1000 km/s, resulting in a large boost factor R (see fig. 3) for a wide range of ϵ_R . The constraints in fig. 4 are derived from observations of the Abell 133 cluster [22]. These limits depend on astrophysical parameters, such as the halo radius, density profile, and magnetic field, and can weaken by a factor of 2, or strengthen by over an order of magnitude.

Other constraints from both INTEGRAL [43] and COMPTEL [44] are derived from the inner region of the galaxy, but due to uncertainty in DM velocity in this region, a detailed recasting is required, which we do not perform. Moreover, their limits are generally weaker than those from XMM-Newton, except for DM masses of a few MeV.

Figure 4 presents the predicted annihilation cross-section $\langle \sigma v \rangle_{220} \equiv \langle \sigma v \rangle (v_{\text{DM}} = v_\odot)$ that satisfies the relic density constraint for different values of ϵ_R , compared to the limits extracted from XMM-Newton ($m_\chi < 5$ GeV), **Leo T** ($m_\chi < 1.3$ GeV), Fermi-LAT (for $m_\chi > 2$ GeV), and MeerKAT ($m_\chi > 5$ GeV), assuming annihilation into e^+e^- (top panel) or $\mu^+\mu^-$ (bottom panel), with $\gamma_R = 10^{-12}$. For $\epsilon_R = 10^{-6}$, the maximum resonant enhancement occurs at v_\odot , leading to strong XMM-Newton and MeerKAT constraints that exclude DM over the entire mass range. For $\epsilon_R = 10^{-5}$, XMM-Newton pro-

vides the most stringent constraint for $m_\chi < 5$ GeV, but does not exclude the relic-density compatible region. Notably, due to resonance effects, very small couplings are required to reproduce the observed DM abundance, leading to $\langle\sigma v\rangle_{220}$ values much smaller than $3 \times 10^{-26} \text{cm}^3/\text{s}$. MeerKAT rules out the region $m_\chi > 5$ GeV, as it benefits from a large boost factor. The same conclusion applies to both leptonic channels. For $\epsilon_R = 10^{-4}$, the resonance peak shifts to higher velocities, suppressing $\langle\sigma v\rangle_{220}$ and allowing sub-GeV DM to evade current constraints, while MeerKAT excludes DM in the 5–100 GeV range in both leptonic channels. Due to the small DM velocities involved, dwarf galaxies observations do not benefit from a resonance boost and thus fail to constrain resonant DM for any ϵ_R . Similar conclusions hold for DM annihilation into pion pairs. More precisely, for $\gamma_R = 10^{-12}$, we find that the X-ray constraints are evaded for $\epsilon_R \gtrsim 7 \times 10^{-6}$ for muons and $\epsilon_R \gtrsim 8 \times 10^{-6}$ for electrons, at $m_\chi = 1 \text{GeV}$, while radio constraints are evaded for $\epsilon_R \gtrsim 2 \times 10^{-4}$ for both electrons and muons at $m_\chi = 10 \text{GeV}$.